BIOCHEMICAL AND CELLULAR CHARACTERIZATION OF DDX59 HELICASE THAT IS ASSOCIATED WITH ORAL-FACIAL-DIGITAL SYNDROME

A Thesis Submitted to the College of
Graduate and Postdoctoral Studies
In Fulfillment of the Requirements
For the Degree of Master of Science
In the Department of Biochemistry, Microbiology and Immunology
University of Saskatchewan
Saskatoon

By
Kingsley Ekumi

PERMISSION OF USE STATEMENT

I hereby present this thesis in partial fulfilment of the requirements for a postgraduate degree from the University of Saskatchewan and agree that the Libraries of this University may make it freely available for inspection. I further agree that permission for copying of this thesis in any manner, either in whole or in part, for scholarly purposes may be granted by the professor or professors who supervised this thesis or, in their absence, by the Head of the Department or the Dean of the College in which my thesis work was done. It is understood that any copying or publication or use of this thesis or parts of it for any financial gain will not be allowed without my written permission. It is also understood that due recognition shall be given to me and to the University of Saskatchewan in any scholarly use which may be made of any material in my thesis.

Requests for permission to copy or to make other use of material in this thesis in whole or part should be addressed to:

Dean
College of Graduate and Postdoctoral Studies
University of Saskatchewan
116 Thorvaldson Building, 110 Science Place
Saskatoon, Saskatchewan S7N 5C9
Canada

OR

Head of the Department of Biochemistry, Microbiology and Immunology
University of Saskatchewan
107 Wiggins Road
Saskatoon, Saskatchewan,
Canada S7N 5E5

ABSTRACT

DDX59 belongs to the DEAD-box helicase subfamily, and mutations in DDX59 are associated with Oral-facial-digital syndrome (OFDS) that is characterized by malformations of the face, oral cavity, and digits. *DDX59* is one of the sixteen genes that have been reported to be involved in various subtypes of OFDS. Most OFDS-associated proteins are localized primarily to cilia components, and influencing ciliogenesis and ciliary functions. However, the effect of DDX59 mutations in OFDS and their links to ciliogenesis remained unidentified. In this study, we overexpressed the human *DDX59* gene in bacteria and purified the protein using nickel affinity and size exclusion chromatography. The DDX59 protein identity was confirmed by Western blotting analysis using a DDX59 protein specific-antibody. Although the protein sequence and domain organizations suggest DDX59 is an RNA helicase, surprisingly, our *in vitro* helicase assays revealed that DDX59 was ineffective on the RNA substrates tested. In contrast, DDX59 exhibited ATP dependent 3′→5′ DNA helicase activity. Interestingly, the OFDS-associated DDX59 mutations, V367G and G534R, reduced the DNA helicase activity, indicating that the loss-of-function might be the underlying cause of OFDS. Using the CRISPR/Cas9 system, an attempt to generate DDX59 knockout in the human retinal pigmented epithelial (RPE1) cell line resulted in heterozygous knockouts, but not the homozygous knockouts, indicating DDX59 is essential for the cell survival. In spite of retaining only one wild-type allele, our immunofluorescence analysis showed a remarkable decrease in the number of ciliated cells upon DDX59 depletion, suggesting that DDX59 is necessary for the formation of primary cilia. Taken together, we found that DDX59 is an ATP dependent 3′→5′ DNA helicase and an ineffective RNA helicase, and that its loss-of-function might lead to the pathogenesis of OFDS through defective ciliogenesis.

ACKNOWLEDGEMENTS

I would like to express my sincere gratitude to my supervisor Dr. Yuliang Wu. It has been a great honor working with him during the critical part of my Master's degree. I appreciate his allocation of time, ideas, and funding to carry on this research project. His motivation and enthusiasm in helping graduate students was a learning process for me, even during difficult times when pursuing my degree.

I am also thankful to members of the Dr. Wu lab, Dr. Ravi Shankar Singh's comments and suggestions, Manisha Yadav, Shizhuo (Sarah) Yang, and Aanchal Aggrawal for their technical support and discussing research challenges during my thesis. Also, the former members deserve recognition for setting up the CRISPR/Cas9 system: Dr. Manhong Guo and Dr. Venkatasubramanian Vidhyasagar.

I thank my committee members, Dr. Jeremy Lee, Dr. Scot Stone, and Dr. Scot Leary for their encouragement and constructive suggestions during advisory committee meetings, critical reading of the progress reports, and coordinating the path to my thesis defense.

I also like to thank the Department of Biochemistry, Microbiology, and Immunology for awarding me the devolved scholarship during my studies and for creating a well-organized learning environment both in didactic theoretical and practical learning. I am thankful to my friends for their friendship and support during my studies at the University of Saskatchewan.

Finally, I thank my wife, Hanna Ekumi, and my kids Tianna Ekumi, Riku Ekumi, and Rauli Ekumi, for their kind and lovely support and encouragement throughout the studies. I am also thankful to my brothers and sisters, especially my sister Nicolette Ekumi, for their support. Lastly, I thank the almighty God for his grace and spirit.

LIST OF ABBREVIATIONS

ADP	Adenosine diphosphate
ADP-BeFx	Adenosine diphosphate-beryllium Fluoride
AMP-PNP	Adenylyl-imidodiphosphate
ATP	Adenosine triphosphate
ATP-γ-S	Adenosine 5′-[γ-thio] triphosphate
BBS	Bardet-Biedl syndrome
bp	Base pair
BSA	Bovine serum albumin
CRISPR	Clustered regularly interspaced short palindromic repeats
CV	Column volume
DAPI	4',6-diamidine-2'-phenylindole dihydrochloride
Dhh	Desert hedgehog
DMEM	Dulbecco's modified eagle’s medium
DNA	Deoxyribonucleic acid
dsDNA	Double strand DNA
dsRNA	Double strand RNA
EMSA	Electrophoretic mobility shift assay
F	Tension force
FBS	Fetal bovine serum
Hh	Hedgehog
IFT	Intraflagellar transport
Ihh	Indian hedgehog
INPP5E	Inositol polyphosphate 5-phosphatase
JBTS	Joubert syndrome
LB	Lysogeny Broth
MKS	Meckel-Gruber syndrome
mRNA	messenger Ribonucleic acid
NPHP	Nephronophthisis
NTP	Nucleoside triphosphate
OFDS	Oral Facial Digital Syndrome
PAM	Protospacer adjacent motif

PBS	Phosphate-Buffered Saline
PBS-T	Phosphate-Buffered Saline-Tween 20
PCR	Polymerase chain reaction
PIPKIγ	Phosphatidylinositol kinase gamma
PMSF	Phenylmethylsulfonyl fluoride
pre-mRNA	precursor-messenger RNA
PS	Penicillin-Streptomycin
RNA	Ribonucleic acid
RPE1	Retinal pigment epithelia cell line
SF	Superfamily
Shh	Sonic hedgehog
SLS	Senior-Løken syndrome
TBE	Tris-borate-EDTA
TTBK2	Tau tubulin kinase 2
ZNHIT	Zinc finger HIT

TABLE OF CONTENTS

LIST OF TABLES

LIST OF FIGURES

1. INTRODUCTION

1.1. Helicases

Helicases are a large group of enzymes that mediate the nucleoside triphosphate-dependent unwinding of nucleic acid double strands, a necessary step in genome replication, gene expression, recombination, and repair. To effectively unwind a nucleic acid double strand, it is widely considered that helicases first bind to one single strand called the loading strand and translocate along this strand to cause separation of the nucleic acid double strand (Xu, 2003). Studies on the helicase-nucleic acid-binding mechanism have shown that helicases exclusively unwind a nucleic acid double strand containing a single-stranded region in a strictly defined orientation relative to the 5' or 3' end of the nucleic acid double strand. Helicases translocating in the 3'→5' orientation require the single strand on the 3' end **(Figure 1A),** while those translocating in the 5'→3' orientation require the single strand on the 5' end **(Figure 1B)** (Lohman and Bjornson, 1996; Patel and Donmez, 2006; Singleton et al., 2007)**.** However, some helicases have been shown to unwind the nucleic acid double strand irrespective of the single-stranded region (Wong et al., 2013; Xie et al., 2013).

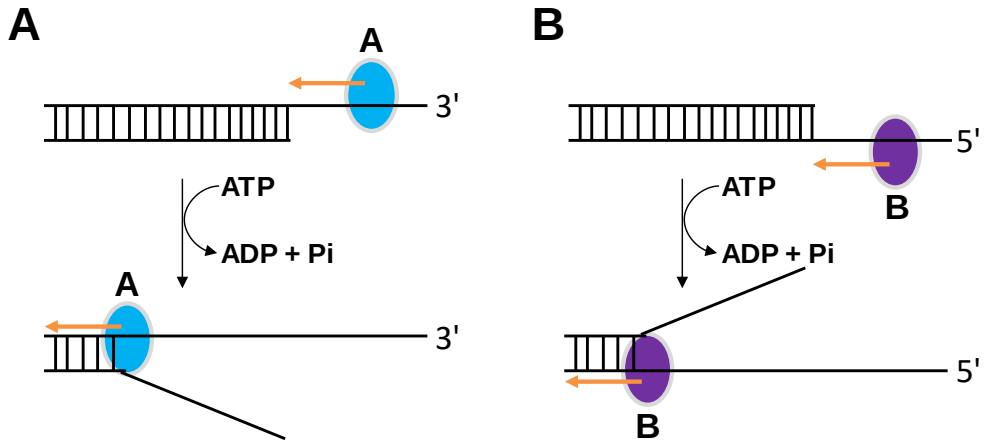

Figure 1. Helicase unwinding directionality.
(A) 3'→5' helicase; (B) 5'→3' helicase. Modified from Xie et al., 2013.

Helicases that unwind DNA substrates are termed DNA helicases while those that unwind RNA substrates are termed RNA helicases, but helicases that unwind both DNA and RNA substrates have been described (Kikuma et al., 2004; Talwar et al., 2017; Tutej et al., 2014; Tuteja et al., 2014). DNA helicases are involved in all aspects of DNA metabolism, such as DNA replication, DNA repair, DNA recombination, gene transcription, and telomere maintenance (Bernstein et al., 2010; Dillingham, 2011). Because of the important roles DNA

helicases play in biological processes, numerous genetic diseases have been linked to mutations in DNA helicases (Croteau et al., 2014; Vannier et al., 2014). RNA helicases are ubiquitously expressed in eukaryotes and function in every step of RNA metabolism from transcription to degradation (Bleichert and Baserga, 2007). While many RNA helicases actively unwind a double-stranded RNA, some function by stabilizing the interaction of a protein or protein-RNA complex (Tanner and Linder, 2001). Due to their ubiquitous presence and functional importance, many RNA helicases are essential for cell viability and are tightly regulated by intramolecular (single protein through oligomerization and/or conformational change) and intermolecular (through protein-protein interaction) mechanisms by changing positions on the RNA and breaking RNA-Protein complexes using the energy derived from ATP binding or hydrolysis (Jankowsky, 2011; Jarmoskaite and Russell, 2014; Linder and Jankowsky, 2011).

1.2. Mechanisms of helicase translocation and unwinding

Differences that exist between the helicase mechanisms of translocation and unwinding include oligomeric state, directionality, translocation rate, step size, ATP-coupling stoichiometry, processivity, and active versus passive. Some helicases can function as monomers, dimers, hexameric, or non-hexameric oligomers (Patel and Donmez, 2006). Some helicases can translocate along the nucleic acid single strand as monomers but lack unwinding activities suggesting that the oligomeric state is critical for helicase mechanism. The step size provides insight into the mechanism of helicase action (Lohman et al., 2008). The helicase step size is defined and measured in different ways. The physical step size is the length of base pairs (*bp*) that a helicase unwinds in one cycle of activity. The mechanical step size is also known as the chemical step size, is the number of *bp* unwind per ATP hydrolysis event. The kinetic step size is measured by a single turnover nucleic acid double strand-unwinding or nucleic acid single strand-translocation experiment and is defined as the average number of *bp* unwound or nucleotides translocated between two successive rate-limiting steps in the unwinding or translocation cycle (Ali and Lohman, 1997; Lucius et al., 2003).

Several studies have established that helicases translocate and unwind a nucleic acid double strand in an ATP-dependent fashion (Enemark and Joshua-Tor, 2006; Gai et al., 2004; Thomsen and Berger, 2009). However, it is unclear how translocation and unwinding processes are coupled (Manosas et al., 2010). Nucleic acid double strand unwinding mechanisms could be classified either as passive or active (Amaratunga and Lohman, 1993;

Betterton and Jülicher, 2005) (**Figure 2**). In the passive mechanism (**Figure 2A**), the helicase interacts with a nucleic acid single strand and translocates unidirectionally and thus stabilizes nucleic acid single strand that has resulted from the transient *bp* opening and closing fluctuations of the upstream nucleic acid double strand. In the active mechanism (**Figure 2B**), the helicase interacts directly with the nucleic acid double strand and facilitates nucleic acid double strand destabilization. The activation energy barrier (ΔG), of an unwinding reaction, is lowered by helicases (Abdelhaleem, 2010; Patel and Donmez, 2006; Wu and Spies, 2013). Factors such as nucleic acid sequence or the tension force (F) on the fork that controls ΔG may affect the unwinding activity of helicases (Donmez and Patel, 2008; Manosas et al., 2010; Schlierf et al., 2019; Syed et al., 2014). In a passive helicase, the unwinding activity is limited by a significant ΔG and is dependent on the nucleic acid GC nucleotide sequence. In an active helicase, the unwinding activity does not have to overcome a significant ΔG and is only independent on the nucleic acid GC nucleotide sequence (Lionnet et al., 2007; Lohman and Bjornson, 1996; Manosas et al., 2010).

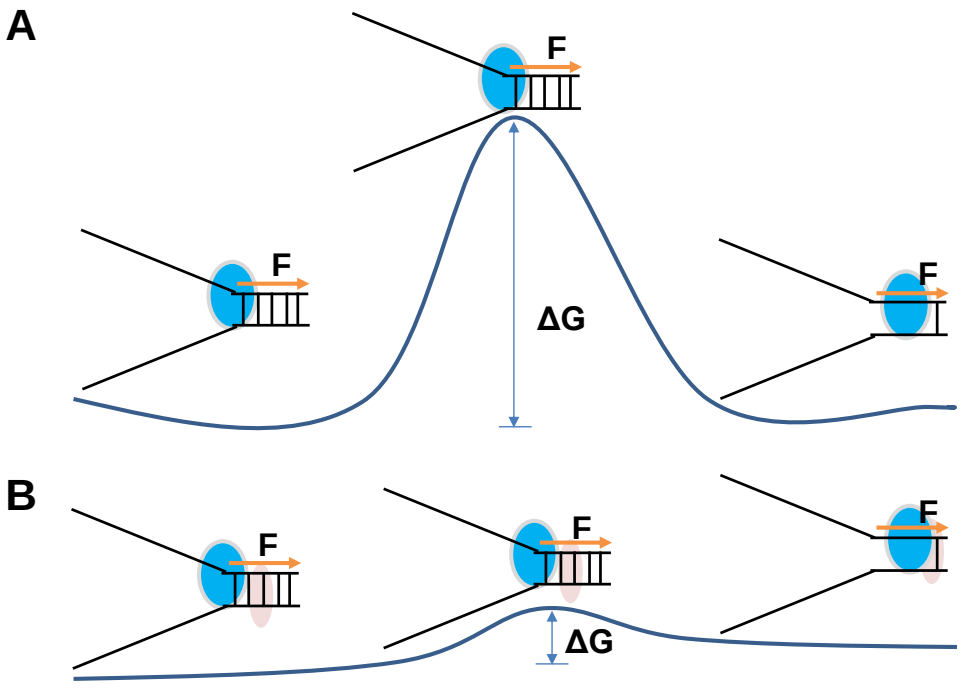

Figure 2. Passive versus active helicase mechanisms.
(A) A passive helicase has to overcome a significant activation energy barrier ΔG to proceed with a nucleic acid double strand unwinding. The rate of unwinding depends on factors such as the nucleic acid sequence or the tension force (F) that destabilizes the nucleic acid double strand fork. (B) An active helicase can destabilize the nucleic acid double strand and effectively reduce the kinetic barrier to fork melting. An active helicase will unwind at a constant rate independent of the nucleic acid sequence. Modified from Manosas et al., 2010.

1.3. Superfamily 2 helicases

Helicases are classified into six superfamilies (SFs), which are designated SF1–SF6 (**Figure 3**) by their characteristic sequence motifs (Gorbalenya and Koonin, 1993). These SFs share structural resemblances in their three-dimensional structures, with RecA1 and RecA2 domains constituting the helicase domain (Jankowsky and Fairman, 2007; Singleton et al., 2000; Subramanya et al., 1996). The RecA-like domain evolved from a 38 kDa structurally characterized protein in bacteria known as Rec A (Horii et al., 1980; Story et al., 1992), which is critical for the repair and maintenance of DNA (Courcelle and Hanawalt, 2003). The SF1 and SF2 helicases are most closely related and classically contain numerous sequence motifs with the NTP binding site found at the interface of the RecA1 and RecA2 domains (Fairman-Williams et al., 2010). Most SF1 and SF2 helicases are suggested to function by the inchworm model mechanisms (Velankar et al., 1999; Singleton et al., 2007; Lee and Yang, 2006; Sarlós et al., 2012). This model includes coordinated and alternated binding to a nucleic acid double strand at different binding sites of the helicase as monomers, dimers or higher order-oligomers (Cheng et al., 2001; Mackintosh and Raney, 2006).

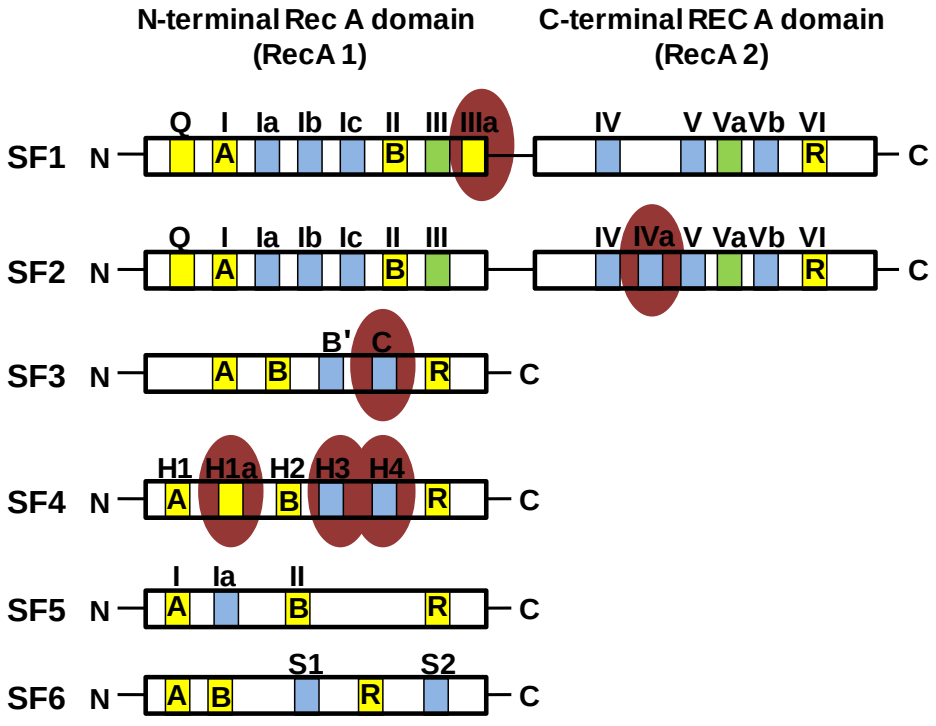

Figure 3. A schematic representation of the core helicase domains of six SFs helicases. The N-terminal RecA 1 and C-terminal RecA2 are represented by white cylinders. Conserved amino acid motifs are colored according to the helicase function. Motifs in yellow are involved in NTP binding and hydrolysis, motifs in green are associated with translocation, and motifs in blue interact with the nucleic acid. Motifs that are unique to specific SFs are highlighted in the red oval. The Walker A (A), Walker B (B), and arginine finger (R) motifs are conserved across all helicase SFs. Modified from Jackson et al., 2014.

Twelve characteristic sequence motifs (I, Ia, Ib, Ic, II, III, IV, IVa, V, Va, Vb and VI) (**Figure 4**) are highly conserved across SF2 helicases (Fairman-Williams et al., 2010), excluding the Q motif that coordinates ATP binding and hydrolysis (Cordin et al., 2004; Tanner et al., 2003). The helicase core of the SF2 helicase consists of two tandemly repeated RecA-like domains, with motifs I, Ia, Ib, Ic, II and III in RecA1 domain and motifs IV, IVa, V, Va, Vb, and VI in RecA2 domain (Fairman-Williams et al., 2010; Jackson et al., 2014; Jankowsky and Fairman, 2007). The RecA1 and RecA2 domains each have their conserved structural fold in the solved structures of SF2 helicases (Mallam et al., 2012; Sengoku et al., 2006; Yao et al., 1999). Motifs I, II, and VI function in ATP binding and hydrolysis; motifs III and Va in coordinating nucleic acid binding and ATP binding; motifs Ia, Ib, Ic, IV, IVa, V, and Vb function in nucleic acid binding (Fairman-Williams et al., 2010).

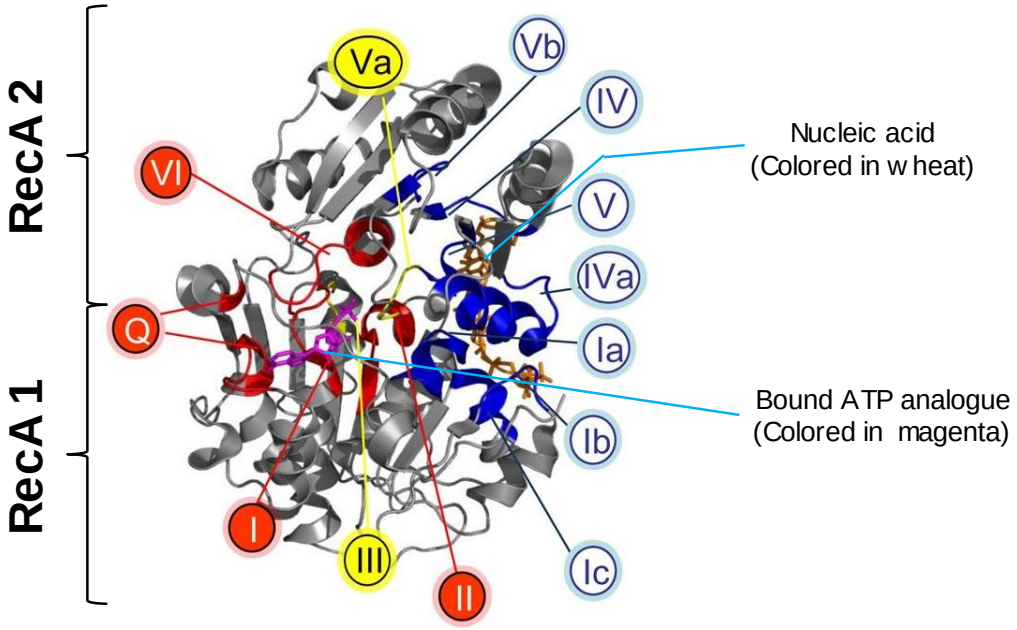

Figure 4. Structural organization of the helicase core of SF2 helicases.
Position of the characteristic motifs in three-dimensional structures of SF2 protein Vasa (*Drosophila*, PDB: 2DB3). Characteristic sequence motifs are colored according to their predominant biochemical function: red, ATP binding and hydrolysis; yellow, coordination between nucleic acid and NTP binding sites; blue, nucleic acid binding. Modified from Fairman-Williams et al., 2010.

The SF2 helicases are the largest and most diverse of the SF helicases and are further divided into ten subfamilies, including DEAD-box, DEAH/RHA, NS3/NPH-II, Rad3/XPD, RecGL, RecQL, RIG-I-like, Swi/Snf, Ski2L and type I restriction enzyme families by sequence annotation (Fairman-Williams et al., 2010; Jankowsky and Bowers, 2006; Jankowsky and Fairman, 2007). The SF2 helicases are involved in diverse cellular functions including transcriptional regulation (Fuller-Pace, 2006), DNA repair (Edwards et al., 1999),

chromatin remodeling (Mashtalir et al., 2018) and every step of RNA metabolism from transcription to degradation (Kawaoka et al., 2004). Mutations in SF2 helicases underline a variety of human genetic (Van Brabant et al., 2000) and inherited diseases (Suhasini and Brosh, 2013). These various diseases can result from the diversities in their additional accessory domains at the C or N terminus of the SF2 helicases. For example, the BLM helicase has a RQC (RecQ C-terminal) domain and HRDC (helicase and RNaseD C-terminal) domain at its C terminus (Swan et al., 2014). Mutations in BLM helicase cause Bloom syndrome, which is characterized by genomic instability with a very high incidence of cancer predisposition (Chester et al., 2006; Payne and Hickson, 2009). XPD helicase has an FeS cluster (Rudolf et al., 2006) and an Arch domain (Abdulrahman et al., 2013) at its N terminus. XPD is a component of the eukaryotic transcription initiation factor complex TFIIH (Greber et al., 2019) that is essential in both transcription initiation and nucleotide excision repair (Rudolf et al., 2006; Wolski et al., 2008). Mutations in XPD helicase are associated with three inherited syndromes: Xeroderma pigmentosum, Xeroderma pigmentosum with the Cockayne syndrome, and Trichothiodystrophy (Dubaele et al., 2003; Herrera-Moyano et al., 2014; Suhasini and Brosh, 2013). The RECQL4 helicase is flanked by an accessory RecQ C-terminal region that consists of a zinc-finger domain and a winged-helix domain (Mojumdar et al., 2017). Mutations in RECQL4 are associated with Rothmund-Thomson syndrome and RAPADILINO syndrome (Lindor et al., 2000; Nishijo et al., 2004; Siitonen et al., 2003; Wang et al., 2003). Finally, the DEAD-box helicase DDX1 has a SPRY domain between the Q motif and the N -terminal RecA1-domain (Kellner and Meinhart, 2015). It was found that DDX1 is involved in restricting HIV-1 Rev function in human astrocytes by promoting oligomerization of Rev (Edgcomb et al., 2012; Fang et al., 2004, 2005; Robertson-Anderson et al., 2011).

1.4. The DEAD-box helicases

The DEAD-box helicase is the largest subfamily in the SF2 helicases. It is called because of its characteristic Asp-Glu-Ala-Asp motif within the primary amino acid. These helicases contain the DEAD sequence in motif II, as well as eight other conserved sequence motifs, including two ATP binding domains **(Figure 5)**. They are found in a wide range of organisms, from viruses to higher eukaryotes. Importantly, DEAD-box helicases are involved in many aspects of RNA metabolism (Bourgeois et al., 2016; Sarkar and Ghosh, 2016), such as transcription and pre-mRNA splicing (Honig et al., 2002; Liu, 2002), ribosome biogenesis

(Venema and Tollervey, 1999), RNA degradation (Anderson and Parker, 1998; Honig et al., 2002; Py et al., 1996), and translation initiation (Chuang et al., 1997). Furthermore, DEAD-box helicases are implicated in numerous diseases such as the innate immune response against pathogens (Ahmad and Hur, 2015), inflammatory disease (Kato et al., 2017), and oncogenesis (Bol et al., 2015; Sarkar and Ghosh, 2016).

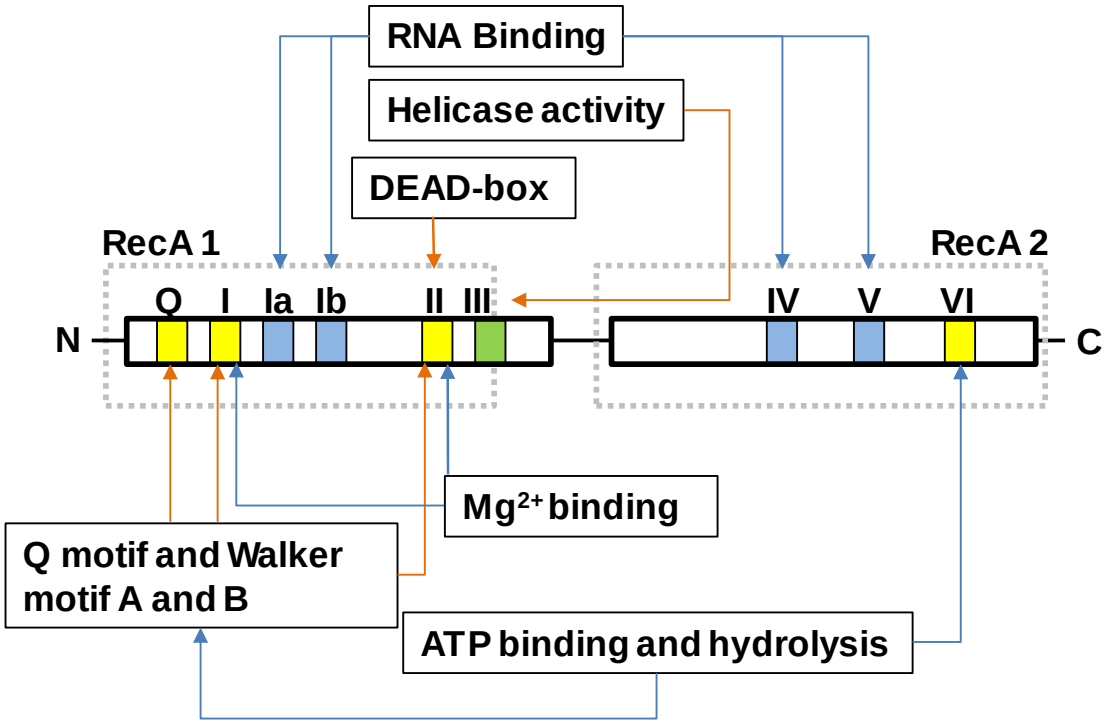

Figure 5. Motif structure of DEAD-box helicases.
DEAD-box helicases are characterized by the presence of an Asp-Glu-Ala-Asp (shown as motif II here). The DEAD-box helicases contain amino-terminal and carboxyl-terminal domains (RecA 1 and RecA 2, respectively) and nine characteristic motifs within these (depicted in the figure as boxes Q and I–VI). The known or proposed functions of each motif are shown. Motif II forms interactions with the β-phosphate and γ-phosphate of ATP through Mg^{2+} and is required for ATP hydrolysis. Modified from Parsyan et al., 2011.

Mutations in multiple DEAD-box helicase genes are frequently associated with diseases and oncogenesis. For example, mutations within functional domains of DDX41 are associated with late-onset hematological myeloid malignancies (Cheah et al., 2017; Polprasert et al., 2015; Quesada et al., 2019; Sébert et al., 2019). Other DEAD-box helicases that have been implicated in human malignancies include DDX3 (Bol et al., 2015), DDX5 (Du et al., 2017), DDX59 (Xie et al., 2019) and DDX17 (Shin et al., 2007). In addition to germline and direct somatic mutations, increased levels of DEAD-box helicases, for example, elF4A1 is detected in multiple cancers, indicating a broad role for DEAD-box helicases in tumorigenesis (Müller-Tidow et al., 2004). DDX11 functions at the interface between DNA repair and sister

chromatid cohesion, and its compromised function is associated with Cohesinopathy in Warsaw breakage syndrome as well as Cornelia de Lange and Roberts syndromes (van der Lelij et al., 2010). A hypomorphic pathogenic variant in DDX3X that affects a region of the protein outside of the critical RNA helicase domain causes intellectual disability with additional neurodevelopmental and neurodegenerative features (Kellaris et al., 2018; Snijders Blok et al., 2015).

1.5. Oral–facial–digital syndromes (OFDS)

Oral-facial-digital syndromes (OFDS) are rare genetic disorders that affect the development of the oral cavity (the mouth and teeth), facial features, and digits (fingers and toes). OFDS has an estimated incidence of one in 50,000 to 250,000, with the majority of the cases being OFDS-I (Franco and Thauvin-Robinet, 2016; Thauvin-Robinet et al., 2006). Researchers have identified at least 13 forms of OFDS subtypes (I-XIII**)** with known causative genes (Gurrieri et al., 2007). The patterns of signs and symptoms distinguish the different subtypes. The physical features of various subtypes overlap significantly, and some types are not well defined (**Table 1)**. The signs and symptoms of OFDS vary widely (Chung and Chung, 1999), with most types involving a problem with the development of the oral cavity, facial features, and digits. Some subtypes are also associated with brain abnormalities and some degree of intellectual disability (Erickson and Bodensteiner, 2007).

Table 1. Classification of OFDS subtypes by clinical features*

Locus	Gene	Inheritance	Oral features	Facial features	Digital features
OFDS I	*OFD1*	X-linked dominant (lethal in males)	Gingival frenulae Lingual hamartomas Cleft/lobulated tongue Cleft palate	Hypertelorism Cleft lip Pseudocleft of the upper lip	Brachydactyly Clinodactyly Preaxial Polydactyly
OFDS II	-	Autosomal recessive	Gingival frenulae Lingual hamartomas Cleft/lobulated tongue Cleft palate	–	Brachydactyly Clinodactyly Pre/postaxial polydactyly
OFDS III	*TMEM231*	Autosomal recessive	Bifid uvula Lingual hamartomas Lobulated tongue Tooth hypoplasia	Hypertelorism Bulbous nose Low-set ears	Postaxial polydactyly
OFDS IV	*TCTN3*	Autosomal recessive	Gingival frenulae Lingual hamartomas Lobulated tongue Cleft palate	Epicanthus Micrognathia Low-set ears	Brachydactyly Clinodactyly Pre/postaxial polydactyly
OFDS V	*DDX59*	Autosomal recessive	Gingival frenulae (rare) Lingual hamartomas	Midline cleft lip Microcephaly	Brachydactyly Clinodactyly Postaxial

					polydactyly Duplication of hallux
OFDS VI	*TMEM216* *C5ORF42* *TMEM138*	Autosomal recessive	Gingival frenulae Lingual hamartomas Lobulated tongue Cleft palate	Hypertelorism Cleft lip	Brachydactyly Clinodactyly Syndactyly Median/Postaxial polydactyly Broad hallux
OFDS VII	-	X-linked dominant	Gingival frenulae Lingual hamartomas Cleft palate	Hypertelorism Cleft lip Asymmetry	Clinodactyly
OFDS VIII	-	X-linked recessive	Gingival frenulae Lingual hamartomas Lobulated tongue Epiglottis hypoplasia	Midline cleft lip Telecanthus Large nose	Bifid thumb Preaxial polydactyly
OFDS IX	*TBC1D32* *SCLT1*	Autosomal recessive	Gingival frenulae Lingual hamartomas Lobulated tongue Cleft palate	Midline cleft lip Synophrys	Brachydactyly Clinodactyly Polydactyly Bifid toes
OFDS X	-	Sporadic	Gingival frenulae Cleft palate	Telecanthus Flat nasal root Retrognathia	Oligodactyly Preaxial polydactyly
OFDS XI	-	Sporadic	Gingival frenulae Cleft palate	Hypertelorism Auricular pits Blepharophimosis	Postaxial polydactyly
OFDS XII	-	Sporadic	Gingival frenulae Bifid tongue Supernumerary teeth	Macrocephaly Hypertelorism	Pre/postaxial polydactyly Club feet
OFDS XIII	-	Sporadic	Lingual hamartomas	Cleft lip	Brachydactyly Clinodactyly Syndactyly
OFDS XIV	*C2CD3*	Autosomal recessive	Gingival frenulae Lingual hamartomas Cleft/lobulated tongue Cleft palate	Telecanthus	Postaxial polydactyly Duplication of hallux
OFDS XV	*KIAA0753*	Autosomal recessive	Lobulated tongue Cleft palate	Hypertelorism	Postaxial polydactyly Broad hallux
OFDS XVI	*TMEM107*	Autosomal recessive	Gingival frenulae Lingual hamartomas Lobulated tongue Cleft palate	Telecanthus Flat nasal root Retrognathia low-set ears	Postaxial polydactyly
OFDS XVII	*INTU*	Autosomal recessive	Gingival frenulae Lingual hamartomas Lobulated tongue Cleft palate	low-set ear Midline cleft lips Retrognathia	Bifid thumbs Postaxial polydactyly
OFDS XVIII	*IFT57*	Autosomal recessive	Supernumerary frenulae missing incisors	Median cleft lip,	Brachydactyly Postaxial polydactyly Broad hallux
Unclassified OFDS	*WDPCP*	Autosomal recessive	Lobulated tongue Cleft palate	Median cleft lip	Postaxial polydactyly
Unclassified OFDS	*NEK1*	Autosomal recessive	Lingual hamartomas Hyperplastic frenula Submucous cleft palate Bifid tongue	Maxillary hypoplasia Protruding ears	Brachydactyly Clinodactyly Syndactyly Bifid right hallux

					Broad hallux

*Modified and updated from (Bruel et al., 2017; Franco and Thauvin-Robinet, 2016; Gurrieri et al., 2007).

Clinical manifestation of the oral cavity in the different subtypes of OFDS includes a split (cleft) in the tongue, a tongue with an irregular surface contour (lobulated tongue), and the growth of noncancerous tumors on the tongue (hamartomas). Affected individuals sometimes will display dental irregularities or ceaseless winking of the eyelids (Siebert, 2007; Sugarman et al., 1971). Other known oral features include an opening in the upper lip or roof of the mouth (a cleft lip and palate) (Gómez and Puerto, 2017; Mossey et al., 2009), and a small fold of extra mucous membrane (hyperplastic frenula) that abnormally attaches the lip to the gums (Bhambhani et al., 2015). The clinical facial features often include an opening in the upper lip (a cleft lip), a wide-nose with a broad-flat nasal bridge, and wide-spaced eyes (hypertelorism) (Bruel et al., 2017). Skeletal anomalies of the digits include fusion of the digits (syndactyly), shorter digits (brachydactyly), unusually curved digits (clinodactyly), or the presence of extra digit (polydactyly) as seen in most OFDS (Franco and Thauvin-Robinet, 2016; Gurrieri et al., 2007). The most common subtypes of OFDS distinguished from other subtypes by associating with a genetic disease. For example, OFDS-I associate with polycystic kidney disease (Donnai et al., 1987; Scolari et al., 1997) that is characterized by the growth of multiple cysts within the kidney (Bergmann et al., 2018). Other subtypes of OFDS are associated with neurological abnormalities, particularly affecting the structure of the cerebrum (microcephaly), skeletal anomalies (Annerhn et al., 1984), visual impairment, and cardiac malformations (Bruel et al., 2017; Franco and Thauvin-Robinet, 2016).

1.6. Structure and function of cilia

Cilia are microtubule-based sensory organelles that emanate from the mother centriole and protrude from the cell surface. They are highly conserved throughout evolution and perform a wide array of motile and sensory functions (Eggenschwiler and Anderson, 2007). A ubiquitous appearance of the cilia is observed only in vertebrates (Fliegauf et al., 2007). The ciliary structure consists of a basal body, transition zone, and the axoneme (**Figure 6**). Surrounding the ciliary axoneme is the ciliary membrane, which is an extension of the cell's plasma membrane, but separated from this by the ciliary gate (Gilula and Satir, 1972; Pedersen and Rosenbaum, 2008) that constitutes a diffusion barrier. The basal body originates from a mother centriole on a centrosome that acts as a microtubule-organizing

center and is an extension of the nine-fold ultrastructure pattern of the centriole (Gonçalves and Pelletier, 2017; Nachury et al., 2010). The transition zone is located at the distal end of the basal body (Gonçalves and Pelletier, 2017). At the transition zone, the triplet microtubules of the basal body transition into doublet microtubules to the ciliary membrane (Gonçalves and Pelletier, 2017). Post-translational modifications, such as acetylation, maintain and stabilize the microtubule structure (Song and Brady, 2015). The primary cilia function as chemosensory and mechanosensory organelles in addition to cellular signaling pathways critical in cellular developmental growth (Irigoin and L. Badano, 2011; Pedersen et al., 2012; Zeytinoglu et al., 1996).

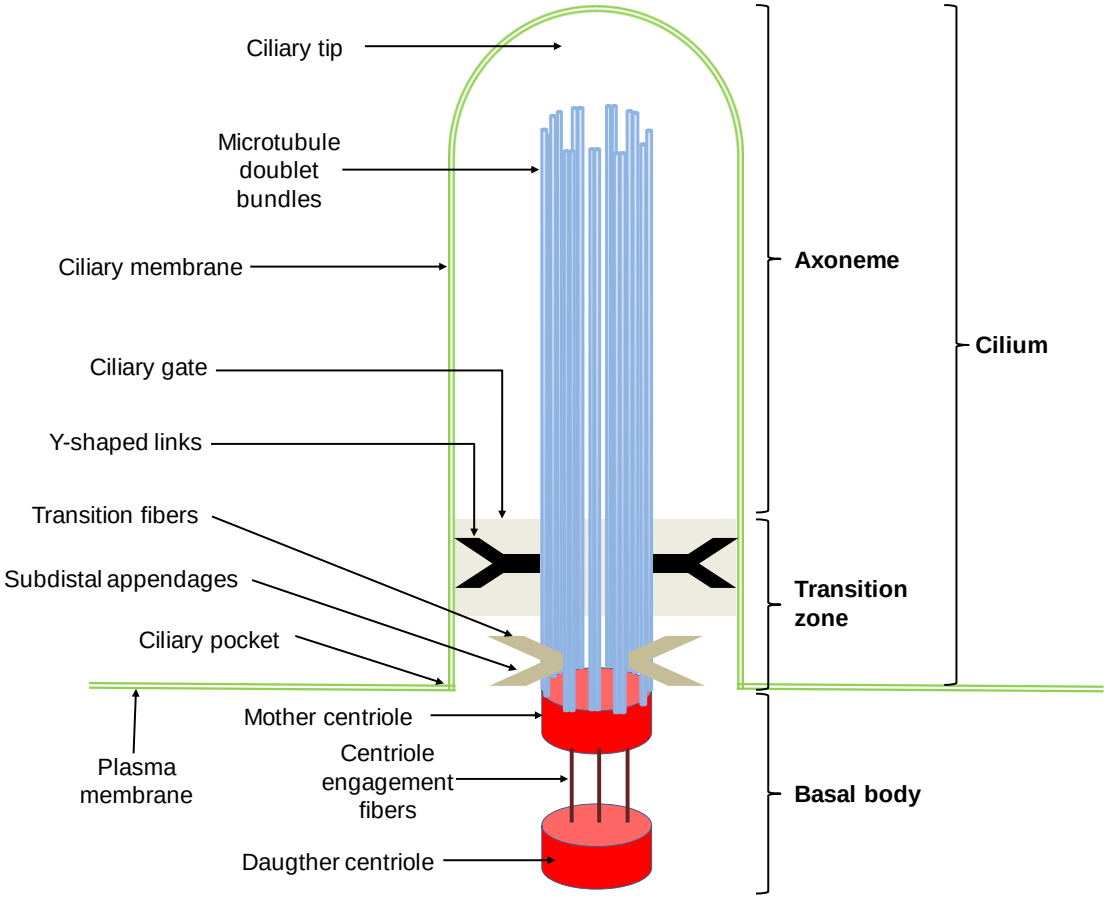

Figure 6. Schematic of primary cilia structure.
The axoneme is bound by ciliary membrane. The mother and daughter centrioles are indicated by the red cylinders. The transition zone is also characterized by Y-shaped links that mediate interactions with the ciliary membrane. Transition fibers extend from the distal appendages of the mother centriole. The permeability barrier called the 'ciliary gate' is indicated in grey. Modified from Malicki and Johnson, 2017.

There are two groups of cilia, motile or immotile, depending on the location and composition of the microtubules. Motile cilia have a (9+2) design of microtubules surrounded by a central pair of microtubules, with doublet microtubules attached to the ciliary membrane

by Y-shaped links characteristics of the transition zone (Gonçalves and Pelletier, 2017). Motile cilia are found in a wide range of organisms from the single-celled green algae *Chlamydomonas reinhardtii* to humans, where they can be present in varying numbers per cell. Some motile cilia are responsible for the movement of single cell, such as spermatozoa that have one flagellum per cell. In vertebrates, fluids and particles are transported by motile cilia across epithelial surfaces of the respiratory tract, oviducts, and brain ventricles (Enuka et al., 2012; Spassky and Meunier, 2017). The immotile cilia, referred to as primary cilia, have a (9+0) design of microtubules in the axonemal structure and lack the central pair of microtubules (Berbari et al., 2009). They lack axonemal dynein and structures that are involved in motility. Primary cilia are mostly present in a single copy per cell when in growth arrest. The primary cilia function to transmit and receive extracellular signals required for regulating cellular signaling pathways, such as hedgehog (Hh) and Wnt signaling (Goetz and Anderson, 2010; Wallingford and Mitchell, 2011).

1.7. Ciliary hedgehog signaling

The Hh pathway was first identified through genetic analysis of *Drosophila* embryogenesis (Nüsslein-volhard and Wieschaus, 1980). The Hh ligand is a morphogen that functions in a concentration gradient manner during tissue development (Mullor and Guerrero, 2000; Strigini and Cohen, 1997). The Hh morphogens are Hh in flies (Nüsslein-volhard and Wieschaus, 1980), and Sonic hedgehog (Shh) (Echelard et al., 1993), Indian hedgehog (Ihh) (Marigo et al., 1995) and Desert hedgehog (Dhh) (Tate et al., 2000) in mammals. In vertebrates, the Hh signaling regulates cell fate and stem cell maintenance in tissues and organs (Ingham and McMahon, 2001; Hooper and Scott, 2005). Severe developmental defects in vertebrates are associated with defective Hh signaling (Bale, 2002; Rohatgi and Scott, 2007).

The major role of the mammalian Hh pathway involves a sequence of repressions and interactions events (**Figure 7**). The transmembrane proteins Smoothened (Smo) and patched (Ptch1) and the Gli transcription factors are central to the pathway. Smo is inhibited by Ptch1 in the absence of a Hh ligand, and is activated in the presence of the Hh ligand (Ingham and McMahon, 2001; Rohatgi and Scott, 2007; Wang et al., 2007). The regulation of Smo leads to the transcriptional activation or repression of Hh signaling genes through the Gli transcription factors, Gli1-Gli3. Gli1 and Gli2 function as modified transcriptional activator

Gli^A, while Gli3 functions in its full length or truncated N-terminal fragment as a repressor Gli^R (Rohatgi and Scott, 2007).

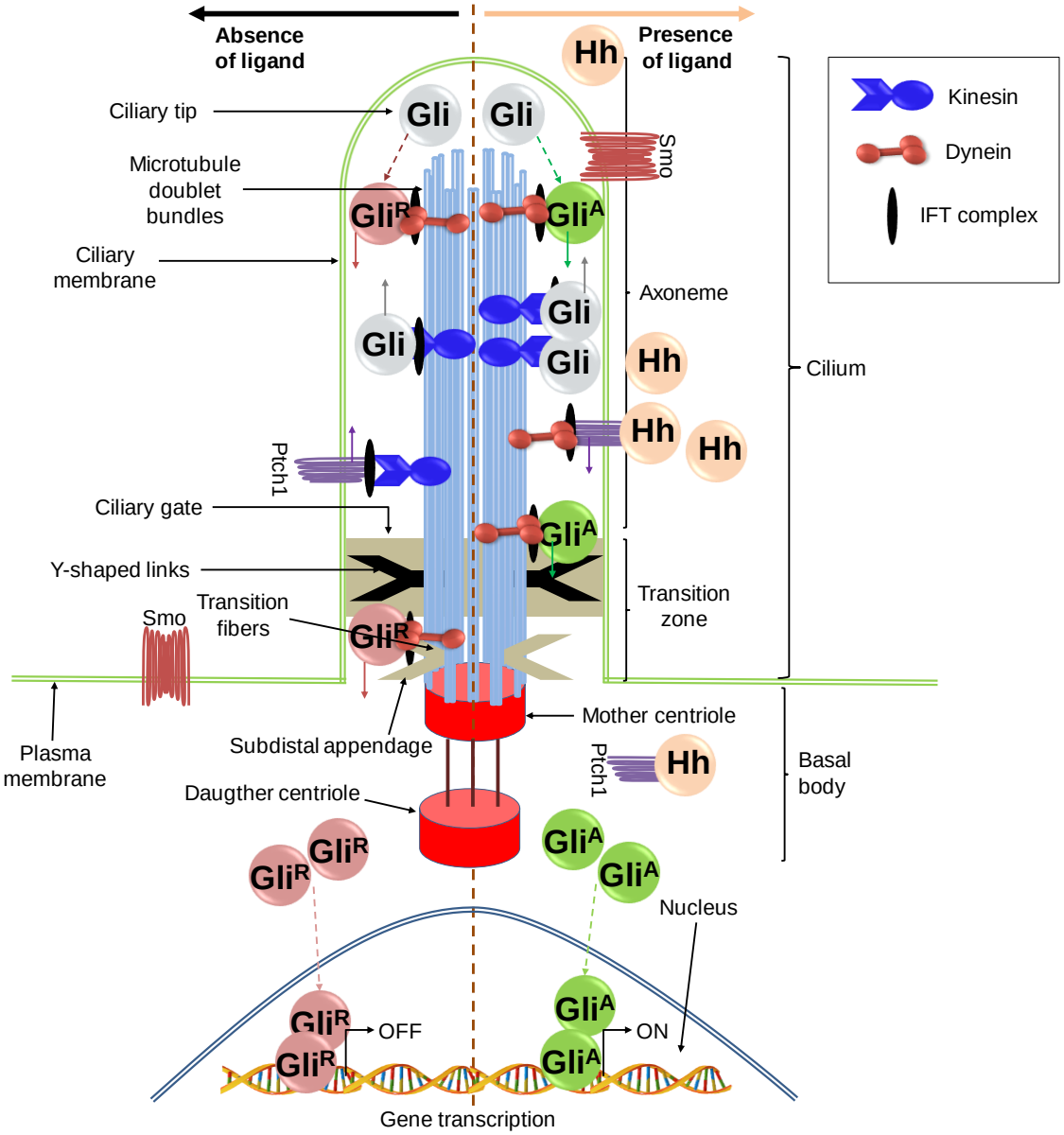

Figure 7. Basic structure of the mammalian hedgehog pathway.
In the absence of Hh (left), Gli protein is converted to its repressor form (Gli^R). Also, in the absence of Hh, Ptch1 is localized to the ciliary membrane, and Smo is kept out of the cilium. In the presence of Hh (right), Gli protein levels increase in the cilium and Gli is processed into the activator form (Gli^A) for transport out of the cilium and into the nucleus, where it activates Hh target genes. In the presence of Hh, Ptch1 moves out of the cilium and Smo moves into the cilium, where it promotes formation of the activator form of Gli (Gli^A). Kinesin 2 moves the intraflagellar transport (IFT) complex and its cargo (e.g., Gli, Ptch, and Smo) toward the ciliary tip. Dynein 2 moves the IFT complex and its cargo toward the cell body. Modified from Hassounah et al., 2012.

1.8. Ciliogenesis

Ciliogenesis is the process of ciliary formation and occurs in resting cells. Ciliary formation is initiated during cell cycle exit at G1 or G0 phase upon mitogen deprivation or differentiation signals, and disassembly takes place upon cell cycle re-entry (Sánchez and Dynlacht, 2016; Yoshimura et al., 2007). Ciliogenesis can be recapitulated in cell lines, such as RPE1 and 3T3 fibroblasts cells by culturing under serum starvation conditions (Pugacheva et al., 2007; Tucker et al., 1979). Ciliogenesis can be divided into four distinct phases (**Figure 8**) that include all the events that occurred before and after the basal body anchors at the plasma membrane.

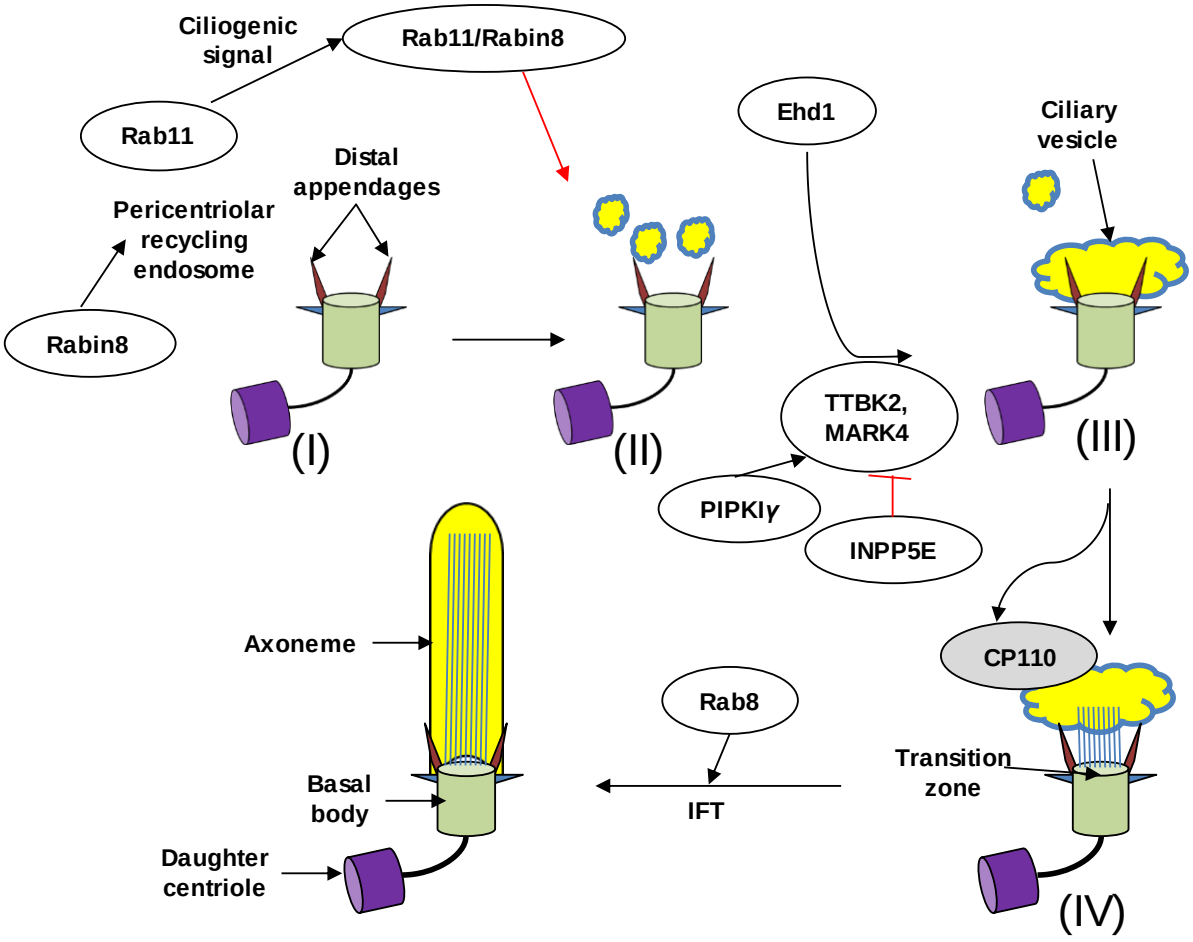

Figure 8. Key players and events in cilium formation.
Cilium formation proceeds through a series of orchestrated and well-defined stages (labelled I–IV). Modified from Sánchez and Dynlacht, 2016.

The mother centriole transforms into a modified centriole called the basal body, which serves as a nucleating site from which the axoneme elongates (Bettencourt-Dias et al., 2011; Rosenbaum and Witman, 2002). Initiation of ciliary formation is marked by the recruitment

and accumulation of small cytoplasmic vesicles around the distal appendages of the basal body, where they seem to anchor (Kobayashi et al., 2014; Lu et al., 2015; Schmidt et al., 2012). These small cytoplasmic vesicles are called distal appendage vesicles, it is assumed they originate from the Golgi apparatus and recycling endosomes. The recruitment and accumulation of distal appendage vesicles form a membranous cap called the ciliary vesicle. Further anchoring and maturation of the cilium occur by continuous trafficking of ciliary vesicles, axonemal and membrane proteins (Sánchez and Dynlacht, 2016).

The GTPase Rab8a is involved in maturation and trafficking of vesicles to the mother centriole (Li and Hu, 2011; Stenmark and Olkkonen, 2001; Yoshimura et al., 2007). In growing cells, Rab8a is localized to cytoplasmic vesicles and the Golgi Network but rapidly redistributes to the distal appendages of the mother centriole during ciliogenesis (Li and Hu, 2011; Westlake et al., 2011; Yoshimura et al., 2007). After the formation of distal appendage vesicles, the Ehd1 protein is recruited (Lu et al., 2015), converting these small vesicles to larger and elongating vesicles. Through continuous fusion with Rab8-positive vesicles, they produce the primary cilium membrane (Lu et al., 2015). Rabin8/Rab11 is responsible for activating Rab8 in Rab8-positive vesicles (Westlake et al., 2011), an activation coinciding with the activation of the ciliary assembly program.

The assembly of the distal appendages on the basal body involves the coordinated recruitment of five distal appendage proteins (Cep83, Cep89, Cep164, SCLT1, and FBF1) (Tanos et al., 2013). The asymmetric disassembly of CP110 and its interacting partner Cep97 on mother centrioles may be an obligate event in the initiation of ciliogenesis. Specifically, one distal appendage protein CEP164 has been shown to interact with Rab8a thereby mediating anchoring of ciliary vesicles to the distal appendage (Kobayashi et al., 2014; Schmidt et al., 2012). Further, CEP164 recruits TTBK2 and MARK4 kinases required for the removal of CP110 from the basal body to trigger ciliogenesis (Čajánek and Nigg, 2014). A balance between the activities of PIPKIγ kinase and opposing phosphatase INPP5E modulates PtdIns(4)P and PtdIns(4,5)P_2 levels (Chávez et al., 2015). PtdIns(4)P negatively regulates the recruitment of TTBK2 by modulating its interaction with Cep164 thereby promoting CP110 persistence and suppressing ciliogenesis. The distal appendages are assembly points for the recruitment of IFT proteins and other components required to build the cilium and selectively import proteins through the transition zone, which acts as a ciliary gate to the cilium (Craft et al., 2015; Lechtreck, 2015).

The transition zone is formed after the capping proteins disassembled from the basal body. The cilium is dependent on IFT for assembly, protein transport, and maintenance of the axoneme (Craft et al., 2015; He et al., 2017; Jonassen et al., 2008; Stepanek and Pigino, 2016). The transportation of proteins is bi-directional (Anterograde and retrograde). In the anterograde, the IFT-B complex associates with the motor protein Kinesin-2 and transports proteins along the B tubules towards the cilium tip, while in the retrograde, the IFT-A complex associates with Dynein-2 and returns proteins along the A tubules to the cell body (Lechtreck, 2015; Stepanek and Pigino, 2016). Further elongation and maintenance of the axoneme after the cilium has matured depend on the constant supply of tubulin (Craft et al., 2015).

1.9. Overlap between OFDS and ciliopathies

Defects in primary cilia formation or function underlie a range of developmental disorders collectively termed ciliopathies. Ciliopathies are a set of clinically heterogeneous syndromes with features that include respiratory complications, renal abnormalities, retinal degeneration, structural heart defects, and growth retardation (Hildebrandt et al., 2011). Examples are Bardet-Biedl syndrome (BBS), Senior-Løken syndrome (SLS), Nephronophthisis (NPHP), Meckel-Gruber syndrome (MKS), Joubert syndrome (JBTS) and oral facial digital syndrome (OFDS). The understanding of genotype-phenotype correlation to determine ciliopathies is complex from a single gene to the effect of multiple allelism (Hildebrandt et al., 2011). *NPHP5* is mutated in SLS. NPHP5 interacts with a GTPase regulator and both are localized to the connecting cilia of photoreceptors and primary cilia of renal epithelial cells (Otto et al., 2005). MKS has extreme genetic heterogeneity and displays allelism with other ciliopathies in genes encoding proteins that are structural or functional components of the primary cilium (Hartill et al., 2017; Hildebrandt et al., 2011). Most of the ciliopathies-associated proteins localize to the ciliary compartment, and a common molecular etiology of ciliopathies appears to be the disruption of ciliary formation and function (Hildebrandt et al., 2011).

Like other ciliopathies-associated proteins, the majority of the OFDS-associated proteins identified to date localize to ciliary compartments and influence ciliary formation and function (**Figure 9**). OFD1 contributes to ciliary formation (Ferrante et al., 2006) by acting on the distal centriole to build distal appendages (Singla et al., 2010). Additionally, mammalian cells or a mouse model depleted of OFD1 are defective in Shh and Wnt signaling (Corbit et al., 2008; Singla et al., 2010). TCNT3 and TMEMT231 are components of the MKS protein complex, and their mutations are implicated respectively in Shh signal

transduction (Thomas et al., 2012) and protein localization at the transition zone (Roberson et al., 2015). TMEM216 and TMEM107 are transmembrane proteins localized to the transition zone of growing cilia (Garcia-Gonzalo et al., 2011; Valente et al., 2010) and their depletion induced constant deciliation (Gogendeau et al., 2020). C2CD3 is localized at the distal end of the centriole and required for the assembly of distal appendages and ciliary vesicles anchoring to the mother centriole (Ye et al., 2014). The *DDX59* gene is the latest gene linked to OFDS that affects ciliary function. Together, there is accumulating evidence linking OFDS-associated genes to defects in ciliary formation and function like other ciliopathies-associated genes. The relationship between phenotype and impaired ciliary function, and gene function distinct from ciliary function warrants further studies in OFDS and ciliopathies (Franco and Thauvin-Robinet, 2016).

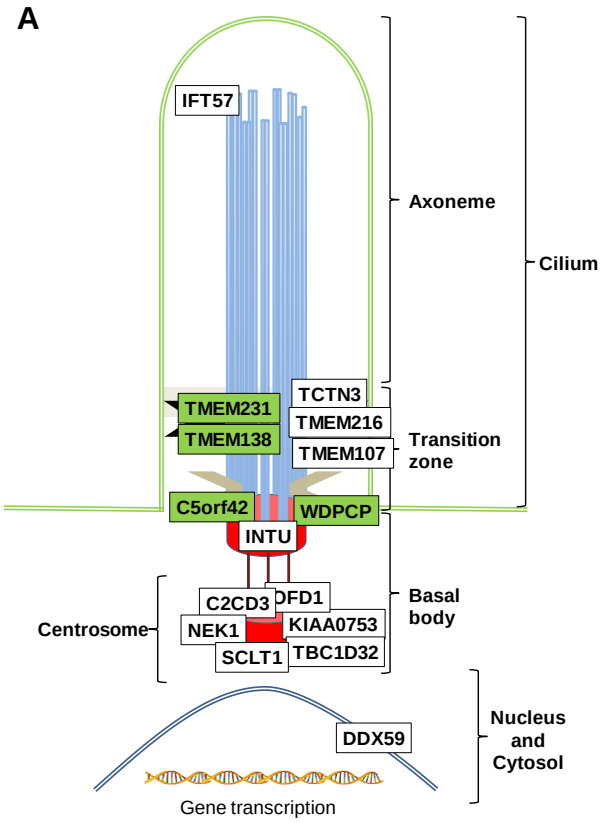

B

Gene	Localization	Cilia/Shh	References
C2CD3	Centrosome, transition fiber	+/+	Hoover et al., 2008
C5orf42	Basal body, transition zone	+/+	Asadollahi at al., 2018
DDX59	Nucleus, cytoplasm	NK/+	Shamseldin et al., 2013
IFT57	Basal body, Axoneme	+/+	Thevenon et al., 2016
INTU	Basal body	+/+	Toriyama et al., 2016
KIAA0753	Centrosome	+/+	Chevrier et al., 2015
NEK1	Centrosome	+/+	Monroe et al., 2016
OFD1	Centrosome	+/+	Ferrante et al., 2001
SCLT1	Centrosome	+/NK	Adly et al.,2013
TBC1D32	Centrosome	+/+	Adly et al.,2013
TCTN3	Transition zone	+/+	Thomas et al., 2012
TMEM107	Transition zone	+/+	Lambacher et al., 2015
TMEM138	Transition zone	+/+	Li et al., 2016
TMEM216	Transition zone	+/NK	Valente et al., 2012
TMEM231	Transition zone	+/+	Li et al., 2016
WDPCP	Basal body, transition zone	+/+	Toriyama et al., 2016

Figure 9. OFDS-associated proteins map to defined primary cilia compartments.
(A) The localization of proteins encoded by OFDS genes is depicted. Sixteen OFDS-associated gene, four genes previously implicated in other ciliopathies (in green) and twelve others (white). (B) The precise cilia localization is defined. Whether Ciliary formation or Shh signaling defect is demonstrated (+) or not known (**NK**). Modified and updated from Bruel et al., 2017; Franco and Thauvin-Robinet, 2016.

1.10. DDX59 as a causative OFDS gene

The *DDX59* gene encodes a relatively uncharacterized member of the DEAD-box helicase protein family (**Figure 10**). By exome sequencing, mutations in *DDX59* were found to be associated with OFDS in 2013 (Shamseldin et al., 2013). In developing mouse embryos, *DDX59* expression is seen in secondary palate, lip, snout region, eye, and limb buds' tissues (Faily et al., 2017; Salpietro et al., 2018; Shamseldin et al., 2013). Patient fibroblast cells from a skin biopsy with *DDX59* mutation (V367G) showed normal nuclear and cytoplasmic localization with significantly reduce protein level of DDX59, and normal ciliation with significantly reduced Shh signaling (Shamseldin et al., 2013). A report on a homozygous frameshift deletion in *DDX59* (F62fs*13) in a family presenting with an OFDS phenotype showed a reduction of mutant cDNA and perturbation of Shh signaling in patient-derived cell lines (Salpietro et al., 2018). However, the exact functions of DDX59 helicase in ciliogenesis and the pathogenesis of OFDS are unclear.

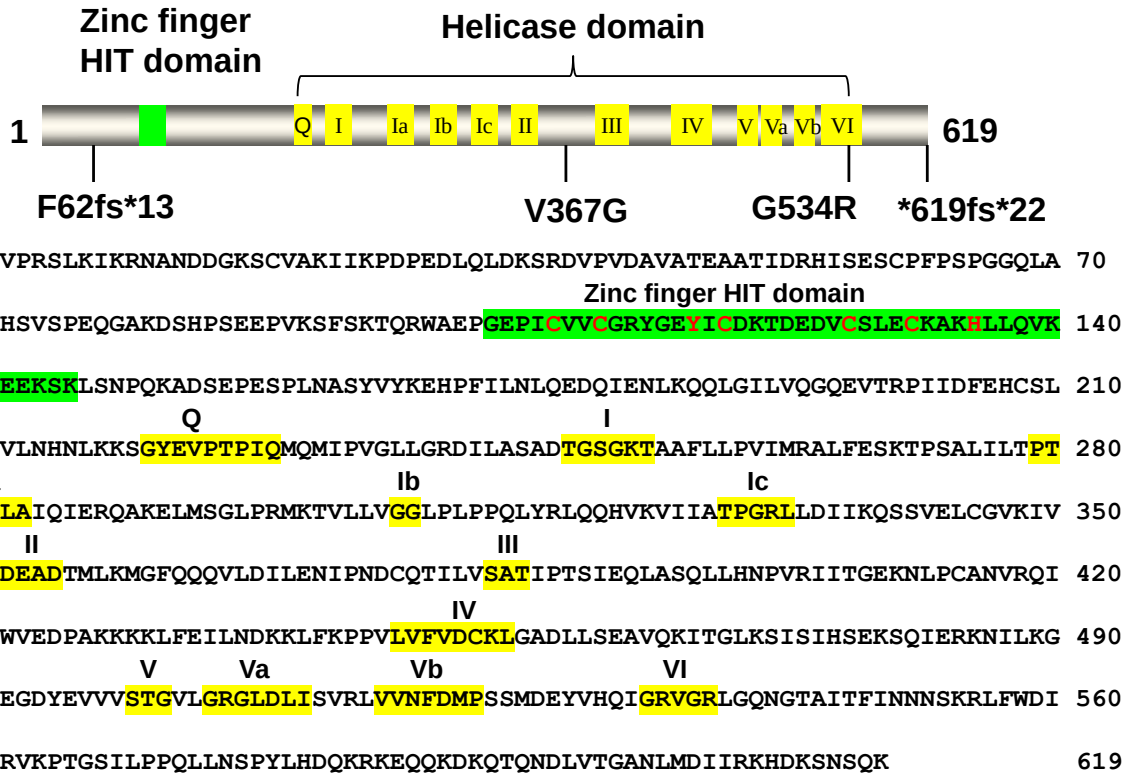

Figure 10. Schematic representation of DDX59 helicase and its primary protein sequence.
Conserved sequence motifs are highlighted in yellow boxes, the zinc finger HIT domain in green box and the OFDS patient mutations are indicated.

2. HYPOTHESIS AND OBJECTIVES

2.1. Rational and Hypothesis

Although DDX59 belongs to the DEAD-box helicase family, the unwinding activity is undescribed experimentally. We hypothesize that DDX59 is a novel RNA or DNA helicase, and defects in its biochemical activities cause OFDS.

2.2. Objectives

2.2.1. To biochemically characterize DDX59 protein activities and examine the effect of OFDS DDX59 mutations.

2.2.2. To investigate the role of DDX59 in the formation of primary cilia in cells.

3. MATERIALS AND METHODS

3.1. Reagents and antibodies

Table 2. List of reagents used in this study

Reagents	Suppliers	Address
2-logDNA ladder, N3200L	NEB	Lawrenceville, Georgia, USA
Acrylamide, 0314	AMRESCO	North York, Ontario, Canada
N,N'-Methylenebisacrylamide, AC164790250hrp	Fisher Scientific	Madison, Wisconsin, USA
Adenosine Triphosphate (ATP), A1852	Sigma-Aldrich	Oakville, Ontario, Canada
Adenosine Diphosphate (ADP), A2754	Sigma-Aldrich	Oakville, Ontario, Canada
Adenylyl-imidodiphosphate (AMP-PNP), A2647	Sigma-Aldrich	Oakville, Ontario, Canada
Adenosine5′-[γ-thio] triphosphate (ATP-γ-S), ALX-480-066-M005	Enzolifesciences	Brockville, Ontario, Canada
Agarose, 5510UB	Gibco	Burlington, Ontario, Canada
Ampicillin, A1593	Sigma-Aldrich	Oakville, Ontario, Canada
Ammonium persulfate (APS), A3678	Sigma-Aldrich	Oakville, Ontario, Canada
Boric Acid, SLBC5554V	Sigma-Aldrich	Oakville, Ontario, Canada
Bovine serum albumin (BSA), A2058	Sigma-Aldrich	Oakville, Ontario, Canada
Bradford protein assay reagent, 500-0013	Bio-Rad	Hercules, California, USA
Bromophenol blue, B0126	Sigma-Aldrich	Oakville, Ontario, Canada
Chloramphenicol, AC227920250	Fisher Scientific	Madison, Wisconsin, USA
Dithiothreitol (DDT), 10197777001	Sigma-Aldrich	Oakville, Ontario, Canada
dNTPs, N0447S	NEB	Mississauga, Ontario, Canada
Dulbecco's Modified Eagle Medium (DMEM), SH30022.01	Sigma-Aldrich	Oakville, Ontario, Canada
EDTA (Ethylenediaminetetraacetic acid), 17892	Fisher Scientific	Madison, Wisconsin, USA
Fetal Bovine Serum (FBS), F6178	Sigma-Aldrich	Oakville, Ontario, Canada
Formic Acid, F0507	Sigma-Aldrich	Oakville, Ontario, Canada
Glycine, BP381-5	Fisher Scientific	Madison, Wisconsin, USA
Glycerol, 123170	Fisher Scientific	Madison, Wisconsin, USA
4-(2-hydroxyethyl)-1-piperazineethanesulfonic acid (HEPES), 391340	Sigma-Aldrich	Oakville, Ontario, Canada
Imidazole, O3196-500	Fisher Scientific	Madison, Wisconsin, USA

Isopropyl β-D-1-thiogalactopyranoside (IPTG), 15528019	Fisher Scientific	Madison, Wisconsin, USA
Kanamycin, 60615	Fisher Scientific	Madison, Wisconsin, USA
Lithium chloride (LiCl)	Fisher Scientific	Madison, Wisconsin, USA
Lysogeny Broth (LB) with agar, L2897	Sigma-Aldrich	Oakville, Ontario, Canada
Methanol, 154246	Sigma-Aldrich	Oakville, Ontario, Canada
Magnesium Chloride ($MgCl_2$), M8266	Sigma-Aldrich	Oakville, Ontario, Canada
Magnesium sulfate ($MgSO_4$), M2643	Sigma-Aldrich	Oakville, Ontario, Canada
3-(N-morpholino) propanesulfonic acid (MOPS), M1254	Sigma-Aldrich	Oakville, Ontario, Canada
Nickel-NTA Affinity beads, 70666	Sigma-Aldrich	Oakville, Ontario, Canada
Non-fat dry milk, 170-6404	Sigma-Aldrich	Oakville, Ontario, Canada
Nonidet P-40 (NP-40), 74385	Sigma-Aldrich	Oakville, Ontario, Canada
N,N,N',N'-Tetramethylethylenediamine (TEMED), 87689	Bio-Rad	Hercules, California, USA
Penicillin-Streptomycin, 084M4778V	Sigma-Aldrich	Oakville, Ontario, Canada
Phenylmethylsulfonyl fluoride (PMSF), P7626	Sigma-Aldrich	Oakville, Ontario, Canada
Protein standard, 161-0374	Bio-Rad	Hercules, California, USA
Protease inhibitor, 05892791001	Roche	Mannheim, Germany
Polyvinylidene difluoride (PVDF), 10600023	GE healthcare	Mississauga, Ontario, Canada
Sodium dodecyl sulfate (SDS), L3771	Sigma-Aldrich	Oakville, Ontario, Canada
Sodium chloride (NaCl), S671-10	Fisher Scientific	Madison, Wisconsin, USA
T4 DNA Ligase, M0202S	NEB	Lawrenceville, Georgia, USA
T4 polynucleotide kinase, M0201S	NEB	Mississauga, Ontario, Canada
Tris, 0826	AMRESCO	North York, Ontario, Canada
Tris(2-carboxyethyl) phosphine, C4706	Sigma-Aldrich	Oakville, Ontario, Canada
Triton-X100, T8787	Sigma-Aldrich	Oakville, Ontario, Canada
Trypsin-EDTA, T4049	Sigma-Aldrich	Oakville, Ontario, Canada
Trypsin, 85450C	Sigma-Aldrich	Oakville, Ontario, Canada
Tryptone, TRP402.205	BioShop	Burlington, Ontario, Canada
TWEEN®20, BP337	Fisher Scientific	Madison, Wisconsin, USA
Q5®Hot Start High-Fidelity DNA Polymerase, M0493S	NEB	Mississauga, Ontario, Canada

Western Blotting detection reagent, RPN2232	GE Health care	Little Chalfont, UK
Xylene cyanol, X4126	Sigma-Aldrich	Oakville, Ontario, Canada
Mouse anti-β-actin (AC-15), A5441	Sigma Aldrich	Oakville, Ontario, Canada
Goat anti-Rabbit IgG (H+L), HRP, 31460	Thermo Fisher Scientific	Madison, Wisconsin, USA
Goat anti-mouse IgG (H+L), HRP, 31430	Thermo Fisher Scientific	Madison, Wisconsin, USA
Mouse anti-DDX59, 514439	Santa Cruz	Dallas, Texas, USA

Table 3. Oligonucleotides used for CRISPR, cloning, and mutagenesis

Primer	**Sequence (5'-3')**	**Used in this study**
DDX59-sgRNA-4T	CACCGGCACAGTTTTCATGC GTGGC	DDX59-sgRNA-4 top strand
DDX59-sgRNA-4B	AAACGGCTGTATAAGACCTC CGATC	DDX59-sgRNA-4 bottom strand
DDX59-sgRNA-gF	GGGTCCAATAAACTAGGAG CAAACC	Forward primer to PCR amplify the genomic DNA surrounding the sgRNA-4 targeted site
DDX59-sgRNA-gR	ATGCATGTCAGAACATTCAA CAGCC	Reverse primer to PCR amplify the genomic DNA surrounding the sgRNA-4 targeted site
DDX59-NdeI-F	GCATCATATGTTTGTTCCAA GATCTCTAAAAATC	Forward primer to PCR amplify the full-length DDX59 gene, with cloning site Nde I for pET28a vector
DDX59-XhoI-R	CATGCTCGAGTTTCTGAGAA TTACTTTTATCATG	Reverse primer to PCR amplify the full-length DDX59 gene, with cloning site Xho I for pET28a vector
DDX59_V367G_F	GTTTTCAACAACAAGGGCTT GACATTTTGGA	Forward primer for DDX59-V367G mutagenesis
DDX59_V367G_R	TCCAAAATGTCAAGCCCTTG TTGTTGAAAAC	Reverse primer for DDX59-V367G mutagenesis
DDX59_G534R_F	GTATGTCCATCAGATTAGAA GAGTAGGAAGAT	Forward primer for DDX59-G534R mutagenesis
DDX59_G534R_R	ATCTTCCTACTCTTCTAATCT GATGGACATAC	Reverse primer for DDX59-G534R mutagenesis

Table 4. DNA and RNA substrates used in this study

Substrate name	Structure or description	Nucleotide sequence (5'→3')
5’ tailed dsRNA (13 bp)	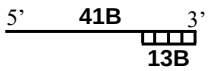	RNA-13B: GCGUCUUUACGGU RNA-41B: AAAACAAAACAAAACAAAACAAA AUAGCACCGUAAAGACGC
3’ tailed dsRNA (13 bp)	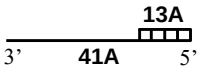	RNA-13A: ACCGUAAAGACGC RNA-41A: GCGUCUUUACGGUGCUUAAAACA AAACAAAACAAAACAAAA
Fork dsDNA (19 bp)	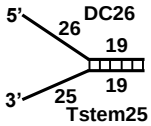	DC26: TTTTTTTTTTTTTTTTTTTTTCCCAG TAAAACGACGGCCAGTGC Tstem25: GCGGTCCCAAAAGGGTCAGTGCTG GCATTTTGCTGCCGGTCACG
5’ tailed dsDNA (19 bp)	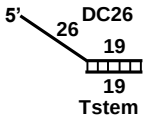	DC26: TTTTTTTTTTTTTTTTTTTTTCCCAG TAAAACGACGGCCAGTGC TSTEM: GCACTGGCCGTCGTTTTAC
3’ tailed dsDNA (19 bp)	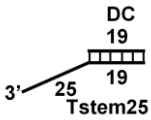	DC: GTAAAACGACGGCCAGTGC Tstem25: GCGGTCCCAAAAGGGTCAGTGCT GGCATTTTGCTGCCGGTCACG
Blunt-end dsDNA (19 bp)	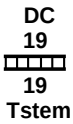	DC: GTAAAACGACGGCCAGTGC TSTEM: GCACTGGCCGTCGTTTTAC
Fork dsDNA (30 bp)	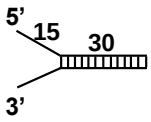	Fork 30/15-T: TTTTTTTTTTTTTTTGGTGATG GTGTATTGAGTGGGATGCATGCA Fork 30/15-B: TGCATGCATCCCACTCAATACA CCATCACCTTTTTTTTTTTTTTT
Fork dsDNA (40 bp)	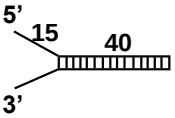	Fork 40/15-T: TTTTTTTTTTTTTTTACGAGCT AAATTAGAGCGACTGCACAACTGTAAGGTCC GT Fork 40/15-B: ACGGACCTTACAGTTGTGCAGTCGCTCT AATTTAGCTCGTTTTTTTTTTTTTTT
Fork dsDNA (50 bp)	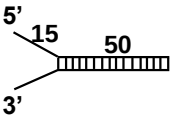	Fork 50/15-T: TTTTTTTTTTTTTTTACGAGCTAAATTAGAGCG ACTGCACAACTGTAAGGTCCGTTGGTCAGCCT Fork 50/15-B: AGGCTGACCAACGGACCTTACAGTTGTGCAGT CGCTCTAATTTAGCTCGTTTTTTTTTTTTTTT

3.2. Plasmid DNA and mutagenesis

The human *DDX59* gene was PCR amplified from the universal human cDNA (636753, Clontech) using primers DDX59-F-NdeI and DDX59-R-XhoI (**Table 3**) and cloned into the NdeI and XhoI sites of the His-tagged pET28a vector (Novagen) for bacterial expression. The V367G and G534R mutations were generated by a QuikChange site-directed mutagenesis kit (Stratagene) according to the manufacturer's instructions using the designed mutagenic primers (**Table 3**). All plasmids were sequenced to ensure the fidelity of all constructs.

3.3. Cell culture

RPE-1 cells (gift from Dr. Laurence Pelletier, the Lunenfeld-Tanenbaum Research Institute, Mount Sinai Hospital, Toronto) were cultured in DMEM F12 or DMEM with 10% FBS, 100 U/mL penicillin/streptomycin, 0.01 mg/mL hygromycin B under 5% CO_2 at 37°C.

3.4. Expression and purification of DDX59 recombinant proteins

The plasmid pET28a-His-tagged-DDX59 was transformed into *E. coli* Rosetta 2 cells (EMD Millipore). The Rosetta 2 cells were cultured in LB medium containing 50 μg/mL kanamycin and 34 μg/mL of chloramphenicol and incubated at 37°C until the OD_{600} reached 0.4. Protein expression was induced by adding 0.3 mM IPTG to the culture and incubated overnight at 16°C. The culture was harvested by centrifugation at 6,000 *g* for 10 min at 4°C. The removal of periplasmic material from the cells was followed using the method described in Magnusdottir et al., 2009. Briefly, the cells were suspended in 5 mL/g of cell mass of hypertonic buffer solution (50 mM HEPES, pH 7.4, 20% sucrose, 1 mM EDTA) and centrifuged at 7,000 g for 10 min at 4°C. The cells were re-suspended in 5 mL/g of cell mass of hypotonic solution (5 mM $MgSO_4$) and incubated for 10 min on ice. Cells were then pelleted by centrifugation at 5000 g for 10 min at 4°C and stored at -80°C until used. The cell suspension was lysed by sonication in buffer A (50 mM HEPES, pH 7.4, 0.15 M NaCl, 0.01% Tween-20 and 10% glycerol) having a final concentration of 10 mM phenylmethylsulfonyl fluoride (PMSF) and protease inhibitor (Roche Applied Science), at 4°C, with five short bursts of 10 sec at intervals of 5 min. The cell debris and inclusion bodies were removed by centrifugation at 45,000 *g* for 30 min at 4°C. Recombinant proteins were subjected to a two-step purification using Nickel Affinity beads (Sigma) and a Sephacryl S-300 HR 16/60 gel filtration column (GE Healthcare). The supernatant was applied to the Ni-NTA beads equilibrated with buffer A; washed with 10 column volumes (CV) of buffer B (50 mM HEPES, pH 7.4, 0.3 M NaCl, 0.01% Tween-20 and 10% glycerol) containing 25 mM

imidazole and eluted with five CV of buffer B containing 250 mM imidazole. The protein fractions were analyzed on reducing SDS-PAGE stained with Coomassie brilliant blue; the fractions containing high protein yield were combined and subjected to size-exclusion chromatography on a Sephacryl S-300 HR 16/60 (GE Healthcare) equilibrated with buffer A. The fractions were collected at a flow rate of 1 mL/min using buffer A. The purity of four protein fractions that eluted in peak 2 of the size-exclusion chromatogram were confirmed on a reducing SDS-PAGE stained with Coomassie brilliant blue and by Western blotting. The protein fractions were pooled and concentrated. The purified protein fractions were snapped frozen in liquid nitrogen and stored at - 80°C until use. The protein concentration was determined using the Bradford method with bovine serum albumin (BSA) used as standard protein concentration.

3.5. Preparation of DNA and RNA substrates

PAGE-purified oligonucleotides were purchased from Integrated DNA Technologies and are listed in **Table 4**. The double-stranded DNA and RNA substrates were prepared as described in (Talwar et al., 2017). Single stranded DNA or RNA oligonucleotides were labeled at the 5′-end with using T4 polynucleotide kinase (NEB) in the presence of [γ-^{32}P]-ATP at 37°C for 1 h. The 5′-end [γ-^{32}P]-labeled single stranded DNA or RNA oligonucleotides were purified using G25 chromatography column (GE Healthcare) and kept at 4°C until use. Annealing of the 5′-end [γ-^{32}P]-labeled single stranded DNA or RNA oligonucleotides with 2.5 fold molar excess unlabeled complementary strand was done in annealing buffer (10 mM Tris–HCl, pH 7.5, 50 mM NaCl for DNA or 10 mM MOPS, pH 6.5, 1 mM EDTA, 50 mM KCl for RNA) by heating at 95°C for 6 min and then gradually cooling to room temperature. Annealed 5′-end [γ-^{32}P]-labeled double-stranded DNA or RNA substrates were purified by PAGE isolation. The final concentration of the annealed 5′-end [γ-^{32}P]-labeled double-stranded DNA or RNA substrate was estimated before use by liquid scintillation counting.

3.6. Helicase assays

The helicase assays were done as described in Talwar et al., 2017. Briefly, the helicase assay reactions were done in a 20 μL mixture containing 40 mM Tris (pH 8.0), 0.5 mM $MgCl_2$, 0.15 mM NaCl, 0.01% Nonidet P-40, 0.1 mM DTT, 1 mg/mL BSA, 2 mM ATP, 2mM $MgCl_2$, 0.5 nM of the specified double-stranded RNA or DNA substrate with the indicated concentrations of DDX59 protein. DDX59 proteins were added to initiate the reaction at 37°C for 30 min or indicated time. 20 μL of 2×stop buffer (17.5 mM EDTA, 0.3% SDS, 12.5% glycerol, 0.02%

bromophenol blue, 0.02% xylene cyanol) containing a 10-fold molar excess of unlabeled oligonucleotide of the 5′-end [γ-32P]-labeled single stranded DNA or RNA oligonucleotide was used to quench the reactions. Helicase assay reactions containing RNA substrates were resolved on non-denaturing 15% (19:1 acrylamide: bisacrylamide) polyacrylamide gels while DNA substrates were resolved on non-denaturing 12% (19:1 acrylamide: bisacrylamide) polyacrylamide gels. All reactions were resolved on the gels for 2 h at 180 V. The results of the helicase assay reactions were visualized using a Phosphor Imager and quantitated using Quantity One software (Bio-Rad).

3.7. Strand annealing assays

The strand annealing assays were done as described in Talwar et al., 2017. The reaction (20 µL) was carried out with 0.5 nM of radiolabeled 13 bp double-stranded RNA. The substrate was denatured first at 100°C for 5 min and then incubated with 0 to 300nM of DDX59 protein at 37°C for 30 min with or without 2 mM ATP. The reaction was quenched by adding an equal volume of 2×stop buffer (17.5 mM EDTA, 0.3% SDS, 12.5% glycerol, 0.02% bromophenol blue, 0.02% xylene cyanol). The mixture was resolved on a 15% native PAGE gel for 2 h at 180 V. The strand annealing assay reactions were visualized using a Phosphor-Imager (Bio-Rad) and analyzed using Quantity One software (Bio-Rad).

3.8. Electrophoretic mobility shift assay (EMSA)

Protein-RNA binding mixtures (20 µL) contained the indicated concentrations of DDX59 and 0.5 nM of the specified ^{32}P-end-labeled RNA substrate in the helicase assay reaction buffer (see above) without ATP. The binding mixtures were incubated at room temperature for 30 min after adding DDX59. After incubation, 3 µL of loading dye (74% glycerol, 0.01% xylene cyanol, 0.01% bromophenol blue) was added to each mixture, and samples were loaded onto native 5% (19:1 acrylamide/bisacrylamide) polyacrylamide gels and electrophoresed at 180 V for 2 h at 4°C using 1×TBE as the running buffer. The EMSA reactions were visualized using a Phosphor Imager and analyzed with Quantity One software (Bio-Rad).

3.9. CRISPR/Cas9 knockout of *DDX59* gene

For genome targeting, *DDX59*-sgRNA-4T (**Table 3**) was designed using the online software http://crispr.mit.edu/. Annealed oligos were cloned into th *Bbs*1 sites of the pSpCas9(BB)-2A-Puro (pX459) vector (#62988, Addgene). The constructs were transiently transfected into RPE1 cells using Lipofectamine 3000 (Invitrogen). 24 h after transfection, puromycin (5 μg/mL) was added into the medium for selection for 14 days. The clones were picked individually and grown in six well plates until confluency, with the cells lysed using RIPA buffer (25 mM Tris, pH 7.4; 150 mM NaCl; 0.5% sodium deoxycholate; 1% NP-40) with 2 mM phenylmethylsulfonyl fluoride (PMSF) and protease inhibitor cocktail (Sigma). Gene knockout was confirmed by Western blot analysis using an anti-DDX59 antibody (#514439, Santa Cruz). Genomic DNA of RPE1 cells was isolated by phenol–chloroform extraction. The targeted region was PCR amplified using primers *DDX59*-sgRNA-gF and *DDX59*-sgRNA-gR for sgRNA-4 (**Table 3**). The PCR products were then cloned into the TOPO-TA vector (Invitrogen) for sequencing.

3.10. Western blotting

Protein concentrations were determined with the Bio-Rad DC protein assay kit (Bio-Rad) using BSA as a standard. Protein samples were reduced by heating at 95°C for 5 min in SDS sample buffer (2% SDS, 10% glycerol, 5% 2-mercaptoethanol, 0.002% bromophenol blue and 0.0625 M Tris HCl, pH 6.8), and the proteins were separated on a 10% SDS-PAGE gel under reducing condition at 120 V for 90 min. For Western blotting, proteins were transferred onto nitrocellulose membranes (Bio-Rad) at 35 V for 16 h at 4°C. After blocking in PBS-T containing 5% nonfat milk for 1 h at room temperature, the membranes were washed in PBS-T and incubated overnight with the appropriate primary antibodies at 4°C. Subsequently, the membranes were washed with PBS-T, and incubated with the appropriate secondary antibodies for 2 h. The membranes were washed in PBS-T and the bands were developed using Chemiluminescent detection using a ChemiDoc MP Imaging System (Bio-Rad).

3.11. Immunofluorescence

Cells were grown to confluence and washed twice with PBS and fixed with 4% paraformaldehyde for 15 min at room temperature. Fixed cells were washed with PBS then blocked with blocking buffer (1% BSA in PBS) at room temperature for 1 h. The cells were washed in PBS, and immunostaining was performed by first incubating cells with a mouse anti-acetyl-α tubulin (1:500, 6-11B-1, Invitrogen) overnight at 4°C. After washing with PBS,

the cells were incubated with Alexa Fluor 488 goat anti-mouse IgG (1:1000, Invitrogen) for 1 h at room temperature. Cells were then washed with PBS and mounted with Prolong Diamond antifade reagent containing DAPI (Invitrogen), and cured at room temperature in the dark for 24 h. Immunofluorescence was performed on a Zeiss LSM 510 META inverted Axiovert 200 M laser scan microscope with a Plan-Apochromat 63×/1.4 oil DIC objective. Images were captured with a CCD camera and analyzed using the LSM Browser software ZEN (Zeiss).

3.12. Statistical analysis

All statistical analyses were performed in Microsoft Excel. Results are reported as mean ± s.d. of at least three independent experiments. Comparisons were analyzed using one-way analysis of variance (ANOVA) test.

4. RESULTS

4.1. Expression and purification of recombinant DDX59 proteins

We overexpressed the recombinant DDX59 protein in Rosetta 2 *E. coli*, and optimized the purification using Nickel affinity and size exclusion chromatography (**Figure 11**). The recombinant 6xHis-DDX59 protein was purified in the first step at the expected molecular weight of 70 kDa (**Figure 11A,** black arrow). However, an unknown protein band (**Figure 11A,** red arrow) appeared just below the DDX59 protein, which might affect subsequent enzymatic assays. To obtain our target protein and exclude the unwanted protein(s), we then pooled fractions 6, 7 and 8 from the nickel purified fractions (**Figure 11A**) and proceeded with size exclusion chromatography to separate the proteins based on size. It resulted in two peaks: one in the void volume (Peak 1) and the other containing DDX59 protein at the expected molecular weight (Peak 2) (**Figure 11B**). Fractions from peak 2 were further analyzed for purity on a SDS PAGE-Coomassie stained gel (**Figure 11C**). The DDX59 protein identity was determined by Western blotting using anti-DDX59 and anti-His antibodies, respectively (**Figure 11 D and E**). These results show that we were able to express and purify DDX59 protein to near homogeneity using nickel affinity and size exclusion chromatography.

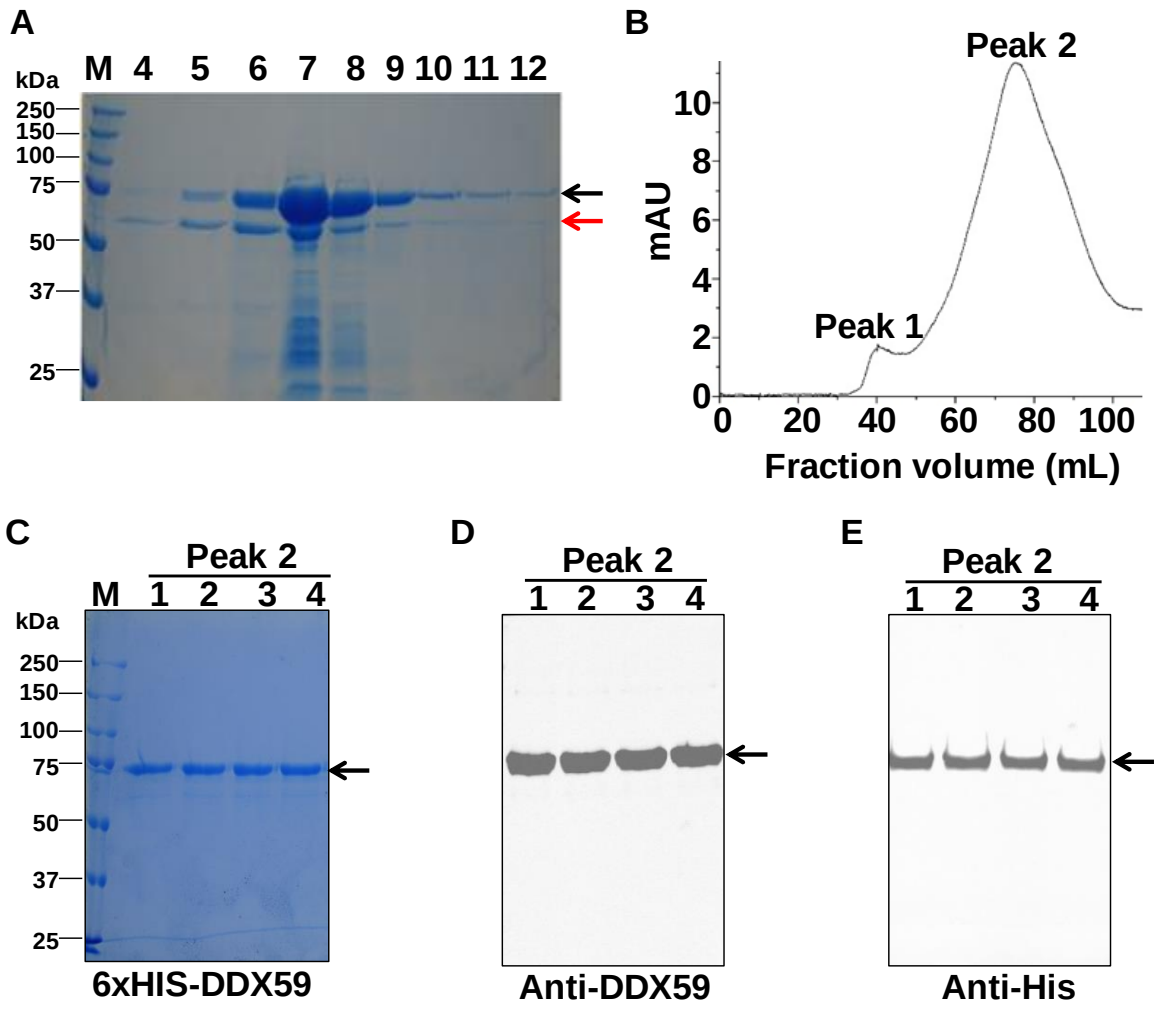

Figure 11. Purification and identification of recombinant DDX59 protein.
(A) A 10% polyacrylamide Coomassie stained gel showing fractions from nickel affinity purification. Recombinant 6xHIS-DDX59 and an unexpected protein are indicated with black and red arrows respectively. M is the protein molecular weight markers. 4-12 are fraction number. (B) Size exclusion chromatography profile of recombinant 6xHIS-DDX59 protein. (C) A 10% polyacrylamide Coomassie stained gel showing four fractions from Peak 2 in B. (D and E) Four fractions shown in Figure 11C were analyzed by Western blotting using anti-DDX59 (D) and anti-HIS (E) antibodies.

4.2. DDX59 is ineffective as RNA helicase *in vitro*

DDX59 is predicted to be a DEAD-box RNA helicase by sequence homology (Shamseldin et al., 2013). To characterize the RNA unwinding activity, we used 5′- (**Figure 12A**) and 3′-tailed (**Figure 12B**) 13-bp double-stranded RNA substrates in helicase assays. We found that DDX59 could not effectively unwind these RNA substrates compared to DDX43 which effectively unwound the double-stranded RNA as previously reported (Talwar et al., 2017). Although we observed a residual unwinding activity with the 3′-tailed 13-bp double-stranded RNA, this activity did not increase with increasing protein concentration (**Figure 12C**). Therefore, we could not show an effective RNA helicase activity for DDX59 protein.

We then asked whether the absence of helicase unwinding activity is due to strong strand annealing activity observed in some helicases (Wu, 2012). We performed strand annealing assays by using the two complementary strands of the 3′-tailed 13-bp double-stranded RNA in the presence and absence of ATP. However, we did not observe any annealing activity in forming the RNA double strand in the absence or presence of ATP (**Figure 12D**).

We hypothesized that the absence of effective unwinding and annealing activity is due to the inability of DDX59 to bind the substrates. To address this, we performed EMSA and found that DDX59 did not bind the 3′- (**Figure 12E**) or 5′-tailed (**Figure 12F**) 13-bp double-stranded RNA substrates.

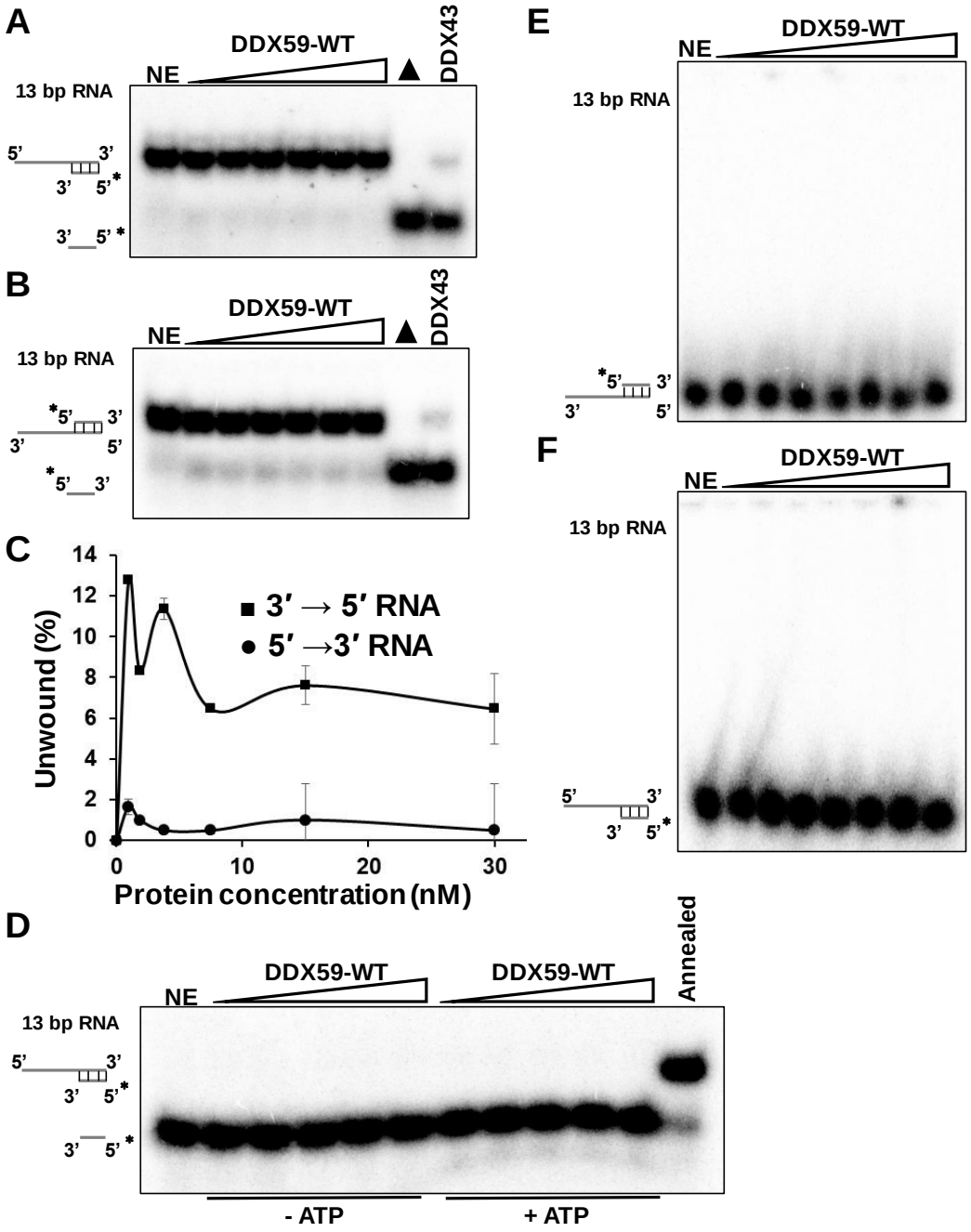

Figure 12. DDX59 does not unwind RNA substrates effectively.
(A and B) Representative 15% polyacrylamide gel showing the helicase activity of DDX59 performed by incubating 0.5 nM 5′-tailed (A) and 3′-tailed (B) 13-bp double-stranded RNA substrate at increasing DDX59 protein concentration (0-30 nM) at 37°C for 30 min. DDX43 protein (300 nM) was used as a positive control. (C) Quantification of helicase activity shown in Figure 12A and B. (D) Representative 15% polyacrylamide gel showing the annealing activity of DDX59 performed by incubating 0.5 nM each of complementary strands of 3′-tailed 13-bp double-stranded RNA substrate at increasing DDX59 protein concentration (0-30 nM) at 37°C for 30 min. (E and F) Representative 5% polyacrylamide gel showing the binding of DDX59 performed by incubating 0.5 nM of 3′-tailed (E) or 5′-tailed (F) 13-bp double-stranded RNA substrate at increasing DDX59 protein concentration (0-30 nM) on ice for 30 min. NE represents no enzyme control and ▲ represents 95°C heated substrate.

4.3. DDX59 is a 3′→5′ DNA helicase

We next asked whether DDX59 possesses DNA unwinding activity. We employed a 19-bp forked double-stranded DNA substrate that has single-stranded DNA at both 5′ and 3′ tails. We found that DDX59 could efficiently unwind the 19-bp forked double-stranded DNA substrate in the presence of ATP in a time- (**Figure 13A**) as well as a concentration-dependent manner (**Figure 13B)**. To define the loading strand and directionality required for DDX59 to initiate DNA unwinding, we used a 3′-tailed (**Figure 13C**), 5′-tailed **(Figure 13D**) and blunt-end (**Figure 13E)** 19-bp double-stranded DNA substrates and found that DDX59 unwound the 3′-tailed double-stranded DNA substrate effectively, but not the 5′-tailed or the blunt-end double-stranded DNA substrate. Collectively, these findings demonstrated that DDX59 is a 3′→5′ DNA helicase.

Next, we examined the DNA helicase activity on variable lengths of double-stranded DNA substrates. For this we used three DNA substrates where the loading strand is kept constant (15 nt) and the length of the double strand is increased progressively from 30 bp, 40 bp to 50 bp (Talwar et al., 2017). DDX59 was able to unwind all substrates (**Figure 13 F, G and H**); however, the unwinding activity for the 40 bp is more effective than the 30 bp and 50 bp substrates, and the unwinding of the 30 bp is less effective than the 50 bp (**Figure 13I**). The discrepancy of these unexpected helicase unwinding activities is due to the difference in the nucleotide sequence composition which might reflect the varied stability of the double-stranded DNA substrates (Manosas et al., 2010).

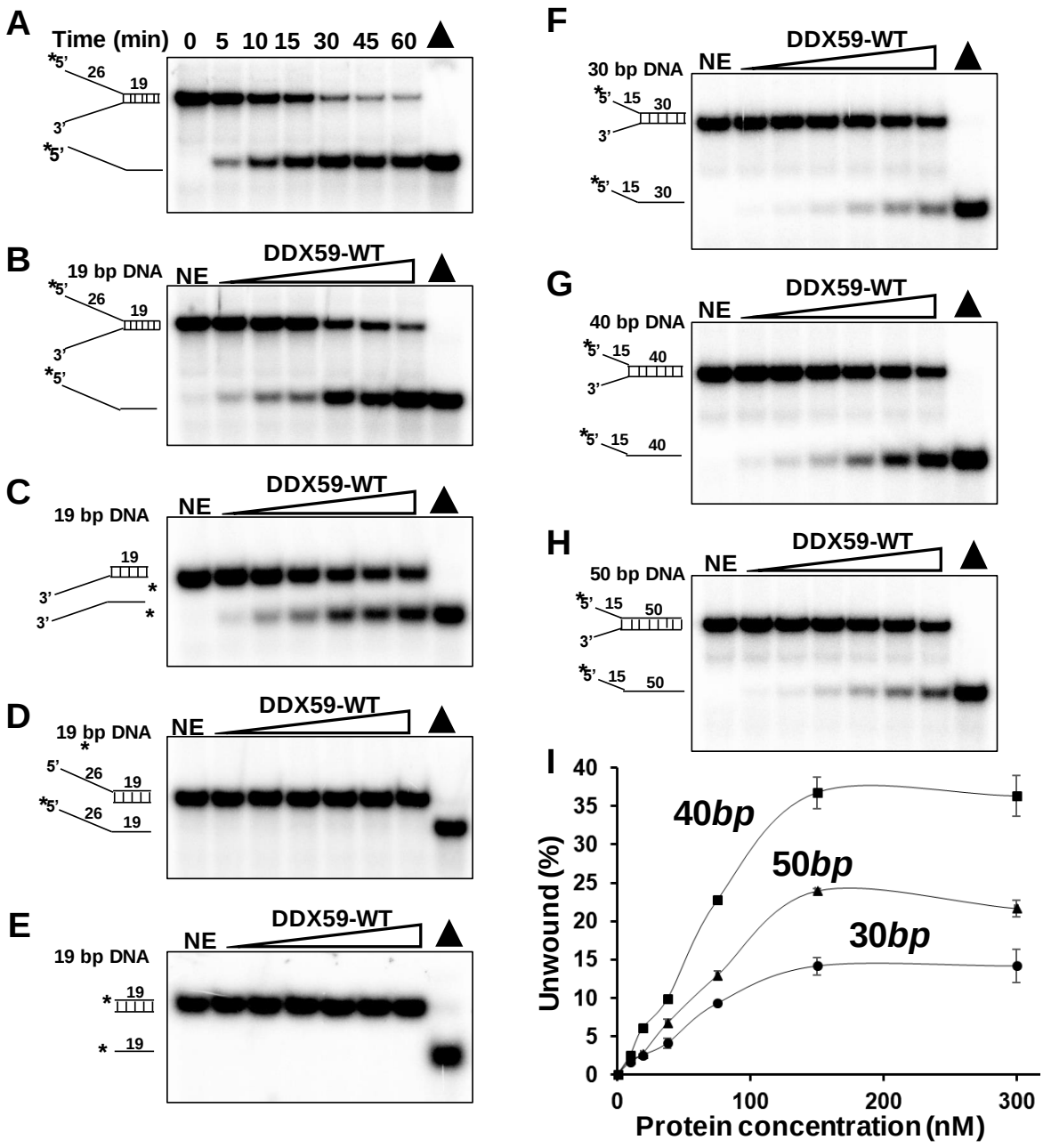

Figure 13. DDX59 shows DNA helicase activity.
(A) Representative 12% polyacrylamide gel showing the helicase activity of DDX59 performed by incubating 0.5 nM 19-bp forked double-stranded DNA substrate with 150 nM DDX59 protein at 37°C for the indicated time. (B-E) Representative 12% polyacrylamide gel showing the helicase activity of DDX59 performed by incubating 0.5 nM 19-bp forked (B), 3′-tailed (C), 5′-tailed (D), blunt-end (E) 19 bp double-stranded DNA substrates at increasing DDX59 protein concentration (0-300 nM) at 37°C for 30 min. (F-H) Representative 12% polyacrylamide gel showing the helicase activity of DDX59 performed by incubating 0.5 nM 30-bp (F), 40-bp (G), and 50-bp (H) forked double-stranded DNA substrate at increasing DDX59 protein concentration (0–300 nM) at 37°C for 30 min. NE represents no enzyme control and ▲ represents 95°C heated substrate. (I) Quantification of helicase activity shown in Figure 13F-H.

4.4. ATP hydrolysis is required for DDX59 unwinding activity

Helicases employ the energy resulting from the ATP hydrolysis cycle to unwind a nucleic acid double strand (Dehghani-Tafti et al., 2019; Wiegand et al., 2019). To determine the NTP required for optimal DDX59 DNA helicase unwinding activity, we employed a standard *in vitro* helicase assay. We found that DDX59 unwound the DNA substrate in the presence of ATP or dATP (**Figure 14A**).

Next, we examined whether DDX59 could unwind a double-stranded DNA substrate with the non-hydrolysable ATP analogs ATP-γS or AMP-PNP. As expected, no unwinding activity was observed with ATP-γS and AMP-PNP compared to the ATP control (**Figure 14B**). Repeated release of an unwound substrate and helicase recycling is critical for efficient nucleic acid double strand unwinding (Wiegand et al., 2019). To mimic a single reaction turnover condition, we used the non-hydrolysable ATP analog ADP-BeFx extensively used in mechanistic and structural studies of other helicases (Chen et al., 2007; Fisher et al., 1995; Kagawa et al., 2004; Liu et al., 2008a). As expected, no unwinding activity was observed with the ADP-BeFx compared to the ATP control (**Figure 14C**). These results demonstrated that ATP hydrolysis is required for DDX59 DNA unwinding activity.

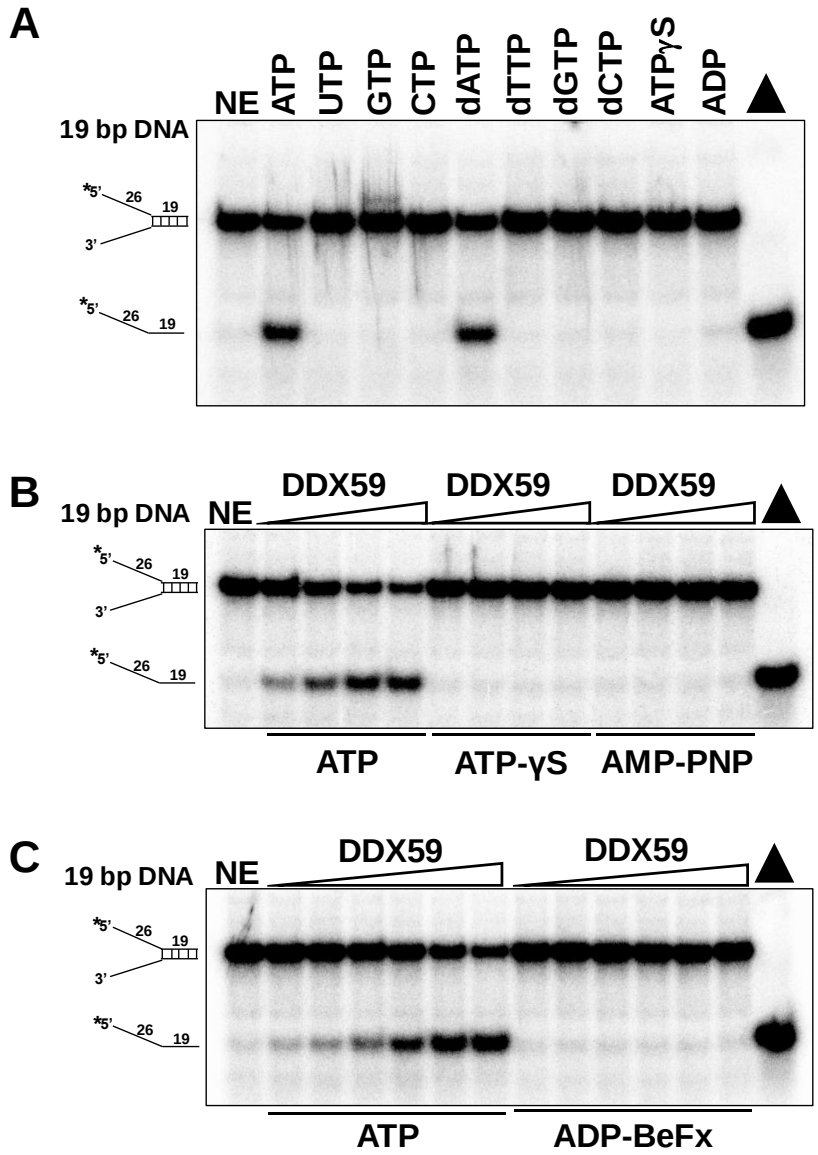

Figure 14. ATP hydrolysis is required for DDX59 unwinding activity.
(A) Representative 12% polyacrylamide gel showing the helicase activity of DDX59 performed by incubating 0.5 nM forked 19-bp double-stranded DNA substrate with 150 nM DDX59 protein at 37ºC for 30 min with various nucleoside triphosphates (2 mM). (B) Representative 12% polyacrylamide gel showing the helicase activity of DDX59 performed by incubating 0.5 nM of forked 19-bp double-stranded DNA substrate with ATP or ATP analogs at increasing DDX59 protein concentration (0–300 nM). (C) Representative 12% polyacrylamide gel showing the helicase activity of DDX59 performed by incubating 0.5 nM of 19 bp forked double-stranded DNA substrate at increasing DDX59 protein concentration (0–300 nM) and 2 mM of ATP or ADP-BeFx at 37ºC for 30min. NE represents no enzyme control and ▲ represents 95 ºC heated substrate.

4.5. DDX59 is necessary for the formation of primary cilia

Most of the OFDS-associated genes identified to date localize to the ciliary compartments and affect the function and formation of primary cilia (Bruel et al., 2017; Franco and Thauvin-Robinet, 2016). Thus, we asked whether DDX59 is involved in the formation of primary cilia. To address this, we generated a *DDX59*-knockout RPE1 cell line using the CRISPR-Cas9 system. The RPE1 cell line is commonly used for cilia studies because they form cilia efficiently and the length of cilia formed is uniform (Spalluto et al., 2013). Upon Western blotting analysis from a whole cell lysate, we found endogenous DDX59 expression disrupted in two clones (**Figure 15A**). The selected *DDX59*-knockout clones were further analyzed for insertion or deletion by TA cloning of genomic PCR products. DNA sequencing revealed that the selected clones were heterozygous, one allele was wild-type, the other had 14 nucleotides deletion, or a single nucleotide insertion (**Figure 15B**). We again attempted to obtain a *DDX59*-homozygous knockout cell line, by repeating transfection, using more serial dilution for the survived cells, or using another cell line (A549), but without success. Importantly we detected a low survival rate (about 40-60%) in the subsequent culture of the *DDX59*-knockout RPE1 cells after puromycin selection, indicating that DDX59 is essential for the survival of RPE1 cells. A similar observation has been reported in other cell lines (HAP1 and KBM7) (Blomen et al., 2015; Yilmaz et al., 2018). *Mahe*, the *Drosophila* homolog of *DDX59,* is essential for survival as well (Salpietro et al., 2018). Importantly, the first three passages of *DDX59*-depleted RPE1 cells had minimal consequences on viability, providing an opportunity window to investigate DDX59 function on ciliary formation.

Following confirmation of the successful depletion of *DDX59* in RPE1 cell lines, we proceeded to investigate the impact of DDX59 on the formation of primary cilia. We visualized the formation of primary cilia by immunofluorescence using an antibody against acetylated α-tubulin, generally considered as a primary ciliary marker (Satir and Christensen, 2007; Shamseldin et al., 2013). We observed a remarkable reduction (about 4-fold) in the number of ciliated cells in the *DDX59*-heterozygous knockout cell line, compared to the wild type cell line (**Figure 15 C and D**). These results indicate that DDX59 is necessary for the formation of primary cilia.

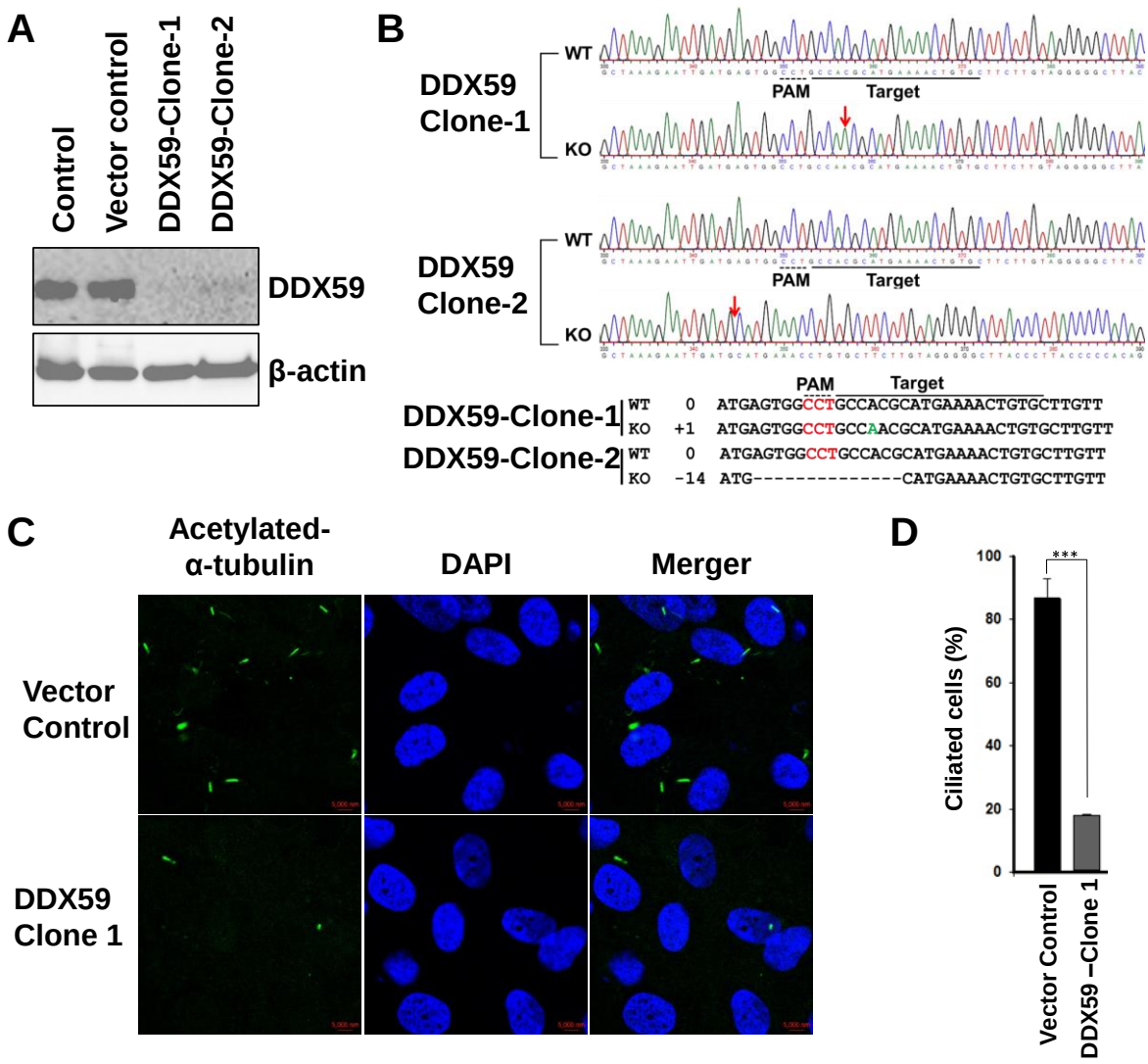

Figure 15. Depletion of DDX59 affects the formation of primary cilia.
(A) Level of endogenous DDX59 protein in whole cell lysate was detected by Western blotting analysis using a DDX59 antibody. β-actin antibody serves as a loading control. (B) Alignment of DNA sequences of the two *DDX59*-heterozygous knockout RPE1 cell lines indicates insertion or deletion in one allele (red arrow). The PAM and target sequences are indicated. (C) The indicated vector control and *DDX59*-heterozygous knockout RPE1 cell lines were immunostained for primary cilia using an acetylated-α-tubulin antibody. The nucleus was stained using DAPI. (D) Quantification of experiments shown in Figure 15C. One hundred cells for each sample were counted. P value was determined by one-way ANOVA. ***$P < 0.0005$.

4.6. DDX59 OFDS mutants have reduced helicase activity

Only four recurrent *DDX59* variants have been reported in OFDS patients (**Figure 16A**) (Faily et al., 2017; Salpietro et al., 2018; Shamseldin et al., 2013). The frame shift F62fs*13 yields a truncated DDX59 protein devoid of most predicted sequence motifs, and the *620fs*22 extends the full-length DDX59 protein by 22 amino acids likely affecting helicase function. Therefore, in this study, we focused on the two missense mutations notably, these residues are conserved from chicken to humans, V367G and G534R (**Figure 16B**).

To determine the effect of these missense mutations on the DNA unwinding activity of DDX59, we purified these two mutant proteins (**Figure 16C**) and performed *in vitro* DNA helicase assays using a 19-*bp* forked double-stranded DNA substrate (**Figure 16D**). Only reduced unwinding activity was observed for the V367G and G534R proteins, when compared to the wild-type protein (**Figure 16E**). These results suggest that the OFDS missense mutants compromise the DNA unwinding activity of DDX59.

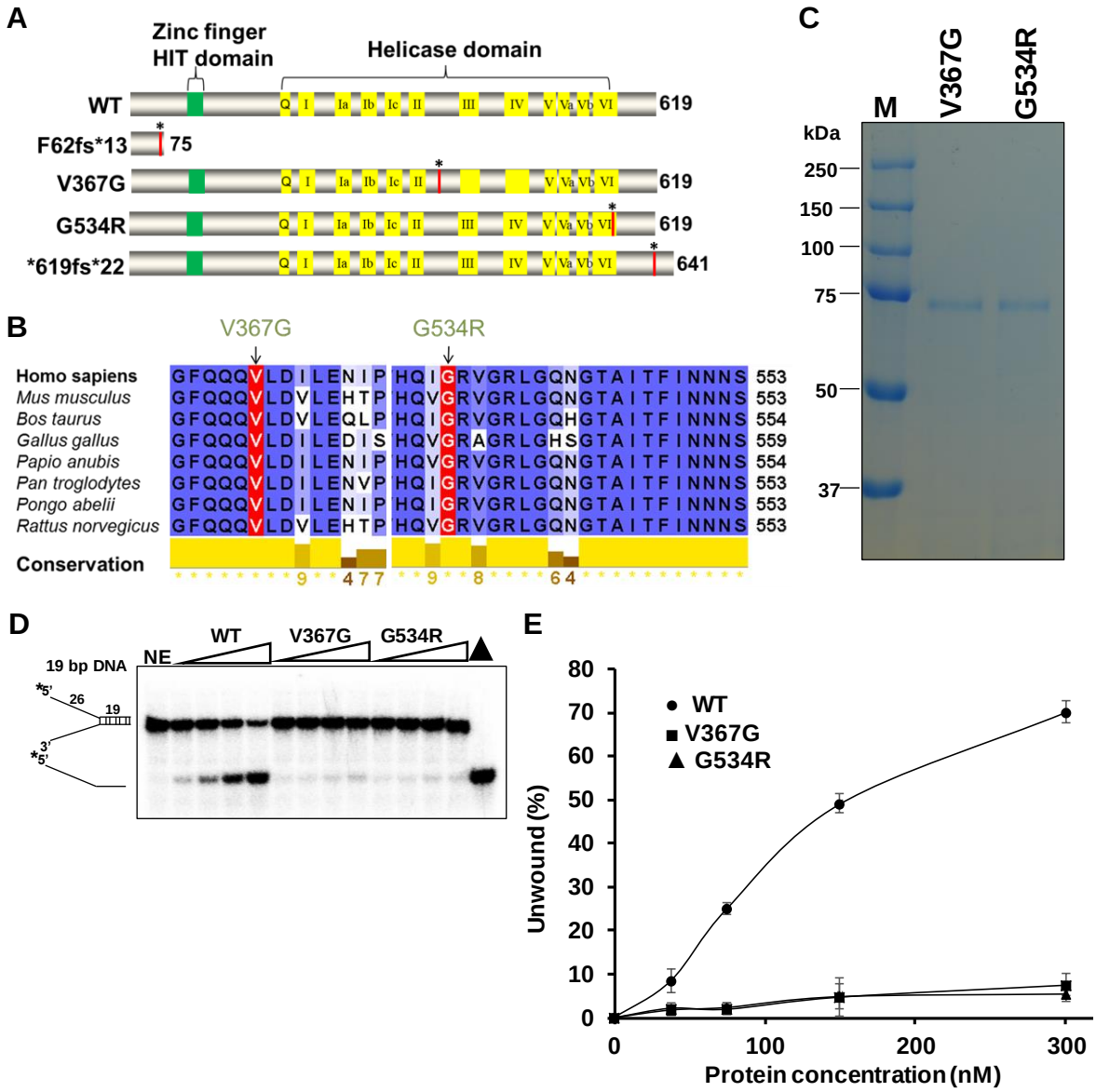

Figure 16. DDX59 mutations in OFDS disrupt the helicase unwinding activity.
(A) Schematic depiction of the wild-type and mutant DDX59 proteins containing individual *DDX59* mutations identified in OFDS. Vertical lines (Red) denote sites of individual missense and frame shift mutations. (B) Evolutionary conservation of the mutated amino acids in DDX59. The conservation is also represented in different shades of gold with numbers below each amino acid indicating the degree of identity from the lowest (1) to the highest (*). The *DDX59* mutations identified in OFDS are highlighted in red. (C) A 10% polyacrylamide Coomassie stained gel showing purified recombinant DDX59 OFDS mutant proteins. (D) Representative 12% polyacrylamide gel showing the helicase activity of DDX59 proteins performed by incubating 0.5 nM of fork 19bp double-stranded DNA substrate at increasing protein concentration (0-300 nM) at 37°C for 30 min. NE represents no enzyme control and ▲ represents 95°C heated substrate. (E) Quantification of helicase activity shown in Figure 16D.

5. DISCUSSION

In this study, we showed that DDX59 is an ATP-dependent DNA helicase and not an effective RNA helicase. DDX59 accomplishes this task by loading on the 3'-overhang of single-stranded DNA. We showed that DDX59 is essential for ciliary formation. We provided biochemical evidence that OFDS-associated DDX59 missense mutations are defective in DDX59 DNA helicase. Collectively, we uncovered the significance of DDX59 in the potential pathogenesis of OFDS, supporting the notion that OFDS is one of the ciliopathies.

5.1. DDX59 is a 3′→5′ ATP-dependent DNA helicase, and ineffective as RNA helicase

Our findings that DDX59 acts as a helicase on double-stranded DNA provide additional insight into the function of DEAD-box helicases in DNA metabolism. DEAD-box helicases display unwinding activities on RNA (Jarmoskaite and Russell, 2011) and some having activities on DNA as well (Kikuma et al., 2004; Pang et al., 2002; Talwar et al., 2017; Tuteja et al., 2014).

Most DEAD-box helicases, including DDX43, Ded1p, and Mss116p, unwind a nucleic acid double strand with no strict directionality. DDX43 unwinds a nucleic acid double strand by a translocation mechanism irrespective of 3′→5′ or 5′→3′ directionality (Talwar et al., 2017; Wu et al., 2019). Ded1p and Mss116p unwind a nucleic acid double strand through local strand separation in either the external strand 3′→5′ or 5′→3′ directionality or in concert with the internal strand (Yang et al., 2007). By comparison, we showed that DDX59 is a 3′→5′ DNA helicase. Our results on the DNA helicase activity of DDX59 on progressively increasing length of the double-strand DNA (**Figure 13I**) is sensitive to the stability of nucleic acid sequence suggestive of a passive helicase (Lionnet et al., 2007; Lohman and Bjornson, 1996; Manosas et al., 2010). Importantly, we further showed that the DNA unwinding activity of DDX59 requires ATP hydrolysis (**Figure 14**).

DDX59 shows ineffective RNA helicase activities *in vitro* for the double-stranded RNA substrates tested in this study, which is unexpected as most DEAD-box helicases are supposed to unwind RNA (Jarmoskaite and Russell, 2011). The varied helicase activity within the DEAD-box family might stem from their accessory domain(s) in their N- and C-termini. DDX59 is one of six human zinc-finger HIT family proteins (ZNHIT1-6) that contain the ZNHIT motif (Verheggen et al., 2015). This motif in ZNHIT6 has no direct RNA binding capacity (Bragantini et al., 2016). Investigation of the role of the ZNHIT motif in DDX59 is

needed. Additionally, this varied helicase activity can be accomplished by oligomerization (Liu et al., 2008a) or the presence of a cofactor (Pang et al., 2002). For example, the founding member of the DEAD-box helicase, elF4A, is thought to use its RNA unwinding capability to unravel secondary structures in mRNA during translation initiation (Abramson et al., 1988; Pause et al., 1993; Ray et al., 1985; Rozen et al., 1990). However, elF4A requires another initiation factor elF4B for enhanced helicase activity (Grifo et al., 1984; Pause et al., 1993; Ray et al., 1985). Although we observed some residual RNA unwinding activities at low concentrations of DDX59, these activities did not conclude effective RNA helicase activity for DDX59 (**Figure 12C**). It is possible to speculate that, like elF4A, DDX59 requires one or more additional cofactors to enhance its helicase activity on double-stranded RNA.

5.2. Role of DDX59 in ciliogenesis as an OFDS-associated gene

Identifying new regulators of cilia will help in providing insight into the molecular mechanism and new animal models for cilia-related diseases. Most of the OFDS-associated genes identified localized to the ciliary compartment with canonical functions in regulating cilia signaling and ciliogenesis (Bruel et al., 2017; Franco and Thauvin-Robinet, 2016).

Previous studies have reported that DDX59 localized to the nucleus and cytosol, with no reports on interference on ciliogenesis (Faily et al., 2017; Salpietro et al., 2018; Shamseldin et al., 2013). Understanding the role of DDX59 in ciliogenesis remains an enigma. One possibility is that DDX59 depletion disturbs the transcription of gatekeeper genes that localize around the transition zone. This could lead to the imbalance in the localization of proteins that control key ciliogenesis processes, such as those involved in the assemble of the transition zone from the basal body. Similarly, it could disturb ciliogenesis via replication initiation factors. For example, the loss of components of the minichromosome maintenance (MCM) protein complex disturbs faithful ciliogenesis by promoting the transcription of a subset of genes, which causes ciliary shortening and centrosome over-duplication (Casar Tena et al., 2019). Of note, DDX59 depletion leads to the downregulation of MCM2 helicase protein levels (You et al., 2017). Thus, our result on the effect of *DDX59* depletion on ciliary formation presents a novel function of DDX59 as an OFDS-associated gene. This new function could arise from an impact on centrosomes. The centrosome is indispensable for ciliogenesis as it comprises the basal body, from which the axoneme elongates (Bettencourt-Dias et al., 2011; Rosenbaum and Witman, 2002).

Increasing evidence suggests an increasing connection between congenital diseases in genes encoding proteins with canonical roles in DNA repair, DNA damage response signaling, or DNA replication with impaired ciliary function (Johnson and Collis, 2016). For example, defects in OFD1 gene that underlie the OFDS-I subtype is known to cause profound impairment in DNA repair functions as well as ciliary formation and signaling; impairments which plausibly contribute to the clinical presentation of OFDS-I subtype (Abramowicz et al., 2017). The DNA damage response apical kinase ATR, often mutated in Seckel syndrome (O'Driscoll et al., 2003), has been shown to regulate ciliary signaling and formation (Stiff et al., 2016). Similar non-canonical function in non-replicating cells is established for MCM2 pre-replicative complex to govern faithful ciliogenesis in resting cells (Casar Tena et al., 2019). Therefore, accumulating evidence demonstrates the complex and mutual functional interactions between DNA damage response, DNA repair, or DNA replication with components that regulate ciliary formation and functions. Thus, DDX59 helicase shown to have a canonical role in DNA replication (You et al., 2017), as an OFDS-associated gene, also confer a role in ciliogenesis.

Collectively, the role of DDX59 in regulating ciliary formation may contribute to the clinical manifestation of DDX59 helicase in OFDS. Whereas, it is difficult to uncouple the influence of the specific cellular defect on ciliogenesis described here from the DNA helicase activities of DDX59; it is in agreement with the cellular characteristics of OFDS-associated genes as ciliopathies-associated genes.

5.3. Molecular pathogenesis of OFDS caused by *DDX59* mutations

Our findings of reduced DDX59 helicase activity shown for the missense mutations may have implications not just in defective helicase, but also in transcriptional regulation. These could have complex adverse impacts during development via altered ciliogenesis that may also influence the clinical features presented by *DDX59* mutations associated with OFDS. The missense mutations biochemically characterized in this study and the nonsense mutations of DDX59 in OFDS are known to impact on cilia through defective Shh signaling (**Table 5**). (Faily et al., 2017; Salpietro et al., 2018; Shamseldin et al., 2013).

Table 5. DDX59 mutations in OFDS and their ciliary or Shh signaling.

DDX59 mutations in OFDS	Shh signaling	Ciliogenesis	Reference
F62fs*13	Yes	Unknown	(Salpietro et al., 2018)
V367G	Yes	Unclear	(Shamseldin et al., 2013)
G534R	Unknown	Unknown	(Shamseldin et al., 2013)
*619fs*22	Yes	Unknown	(Faily et al., 2017)

The OFDS-associated DDX59 patients samples showed reduced mRNA and protein expression without complete defect in nonsense-mediated decay (Faily et al., 2017; Salpietro et al., 2018; Shamseldin et al., 2013). Finally, the two deleterious mutations reported, are presented with a more severe clinical manifestation, including microcephaly and skeletal abnormalities (Faily et al., 2017; Salpietro et al., 2018), and there is mounting evidence that cilia function during skeletogenesis. Because microcephaly is a hallmark of severe structural brain defect, it is in agreement with our findings and also supports the possibility that DDX59 loss of helicase activity mutations might be susceptible to severe clinical features than reduced helicase activity mutations. Of note, the family history of the patient with deleterious F62fs*13 mutation was unremarkable, except for three prior spontaneous miscarriages (Salpietro et al., 2018).

Together, these revelations suggest that these missense mutations are hypomorphic for DDX59 helicase activity, and in each case, the mutations must allow sufficient residual protein function to enable embryogenesis and patient viability explaining the recessive nature of these mutations in OFDS. Thus, the residual helicase activities displayed by the missense DDX59 mutations in OFDS might support ciliogenesis, but insufficient to ensure the correct regulation of cilia function via defective helicase activities. Further investigations of mutations in OFDS are needed to understand their molecular pathogenesis and contribution to OFDS.

6. CONCLUSIONS AND FUTURE DIRECTIONS

In conclusion, we have successfully expressed recombinant DDX59 protein in *E. coli* cells and purified it using Nickel affinity and size exclusion chromatography. Helicase assays showed that DDX59 efficiently unwinds double-stranded DNA with a 3′→5′ direction, and the activity depends on the hydrolysis of ATP. DDX59 ineffectively unwind double-stranded RNA substrates. We have successfully generated RPE1 cell line deficient in DDX59 using the CRISPR-Cas9 system and showed that ciliation in these cells reduced drastically, which is consistent with ciliary formation defect pathogenesis observed for most OFDS-associated genes mutations. We also found that *DDX59* missense mutations in OFDS compromise the DDX59 DNA helicase activities.

We have found that DDX59 is a DNA helicase and deficiency in its helicase activity implicates DDX59 in the pathogenesis of OFDS through defective ciliogenesis and ciliary function. This study biochemically characterized DDX59 for the first time as a DNA helicase

and extends our knowledge on the cellular characteristics of OFDS-associated genes as ciliopathies-associated genes by adding DDX59 to the set of genes in the ciliome database.

In the future, to determine DDX59 and DDX59-OFDS mutants' impact on transcription of genes required for ciliary formation, and their centrosome and ciliary localization, we will: 1) Generate RPE1 model cell line harboring OFDS-associated DDX59 mutations by CRISPR/Cas9 system, 2) Use the RPE1 model cell lines to study the effect on ciliogenesis by counting cilia forming cells and measuring cilia length using high resolution immunofluorescence microscopy, 3) Use the RPE1 model cell lines to compare the cell cycle dependent localization of DDX59 (WT vs. mutant) to the centrosome and cilia using immunofluorescence, and 4) Use the RPE1 model cell lines to compare the differential impact on cilia related genes using transcriptomic approach.

In our current study, we detected a residual RNA helicase activity for DDX59. We suspect that DDX59 might require co-factor(s) to initiate and/or stimulate its unwinding activity on RNA substrate. To identify the protein cofactor, the following objectives need to be realized: 1) To generate inducible HEK293-Fln cell line over-expressing 3xFlag tagged DDX59, 2) To purify 3xFlag tagged DDX59 complexes using affinity chromatography, 3) To separate the different 3xFlag tagged DDX59 protein complexes by size exclusion chromatography, 4) To analyze the RNA helicase activity of the various eluted fractions from size exclusion chromatography, and 5) To identify the potential co-factor by mass spectrometry from the fraction that depicts the highest RNA helicase activity.

To investigate the function of the ZNHIT motif in DDX59, we will: 1) Examine helicase activity of DDX59 mutants by site-directed mutagenesis, 2) Test the DNA helicase activity of ZNHIT motif truncated DDX59, 3) Re-check the RNA helicase and nuclease activity of ZNHIT motif truncated DDX59 using different substrates. Because we found that DDX59 has a weak RNA helicase activity at lower protein concentrations and nuclease activity at higher protein concentrations, and the RNA nuclease activity seems to occur in the U-rich loading strand, and 4) Investigate the RNA and DNA binding activities of ZNHIT motif truncated DDX59.

7. REFERENCES

Abdelhaleem, M. (2010). Helicases: An overview. Methods Mol. Biol. *587,* 1-12.

Abdulrahman, W., Iltis, I., Radu, L., Braun, C., Maglott-Roth, A., Giraudon, C., Egly, J.M., and Poterszman, A. (2013). ARCH domain of XPD, an anchoring platform for CAK that conditions TFIIH DNA repair and transcription activities. Proc. Natl. Acad. Sci. U. S. A. *110,* 633-642.

Abramowicz, I., Carpenter, G., Alfieri, M., Colnaghi, R., Outwin, E., Parent, P., Thauvin-Robinet, C., Iaconis, D., Franco, B., and O'Driscoll, M. (2017). Oral-facial-digital syndrome type I cells exhibit impaired DNA repair; unanticipated consequences of defective OFD1 outside of the cilia network. Hum. Mol. Genet. *26,* 19-32.

Abramson, R.D., Dever, T.E., and Merrick, W.C. (1988). Biochemical evidence supporting a mechanism for cap-independent and internal initiation of eukaryotic mRNA. J. Biol. Chem. *263,* 6016-6019.

Ahmad, S., and Hur, S. (2015). Helicases in Antiviral Immunity: Dual Properties as Sensors and Effectors. Trends Biochem. Sci. *40,* 576-585.

Ali, J.A., and Lohman, T.M. (1997). Kinetic measurement of the step size of DNA unwinding by Escherichia coli UvrD helicase. Science *275,* 377-380.

Amaratunga, M., and Lohman, T.M. (1993). Escherichia coli Rep Helicase Unwinds DNA by an Active Mechanism. Biochemistry *32,* 6815-6820.

Anderson, J.S.J., and Parker, R. (1998). The 3' to 5' degradation of yeast mRNAs is a general mechanism for mRNA turnover that requires the SK12 DEVH box protein and 3' to 5' exonucleases of the exosome complex. EMBO J. *17,* 1497-1506.

Annerhn, G., Arvidson, B., Gustavson, K. -H, Jorulf, H., and Carlsson, G. (1984). Oro-facio-digital syndromes I and II: radiological methods for diagnosis and the clinical variations. Clin. Genet. *26,* 178-186.

Bale, A.E. (2002). Hedgehog signaling and human disease. Annu. Rev. Genomics Hum. Genet. *3*, 47–65.

Berbari, N.F., O'Connor, A.K., Haycraft, C.J., and Yoder, B.K. (2009). The Primary Cilium

as a Complex Signaling Center. Curr. Biol. *19,* 526-535.

Bergmann, C., Guay-Woodford, L.M., Harris, P.C., Horie, S., Peters, D.J.M., and Torres, V.E. (2018). Polycystic kidney disease. Nat. Rev. Dis. Prim. *11,* 3200

Bernstein, K.A., Gangloff, S., and Rothstein, R. (2010). The RecQ DNA Helicases in DNA Repair. Annu. Rev. Genet. *44,* 393-417.

Bettencourt-Dias, M., Hildebrandt, F., Pellman, D., Woods, G., and Godinho, S.A. (2011). Centrosomes and cilia in human disease. Trends Genet. *27,* 307-315.

Betterton, M.D., and Jülicher, F. (2005). Opening of nucleic-acid double strands by helicases: Active versus passive opening. Phys. Rev. E. *71,* 011904.

Bhambhani, N., Gori, J., Masurkar, V., and Thombre, S. (2015). Diode laser in management of tracheobronchial typical carcinoid: A case report with review of literature. J. Clin. Diagn. Res. *9,* 06-07

Bleichert, F., and Baserga, S.J. (2007). The Long Unwinding Road of RNA Helicases. Mol. Cell *27,* 339-352.

Blomen, V.A., Májek, P., Jae, L.T., Bigenzahn, J.W., Nieuwenhuis, J., Staring, J., Sacco, R., Van Diemen, F.R., Olk, N., Stukalov, A., et al. (2015). Gene essentiality and synthetic lethality in haploid human cells. Science *350,* 1092-1096

Bol, G.M., Xie, M., and Raman, V. (2015). DDX3, a potential target for cancer treatment. Mol. Cancer *14,* 188.

Bourgeois, C.F., Mortreux, F., and Auboeuf, D. (2016). The multiple functions of RNA helicases as drivers and regulators of gene expression. Nat. Rev. Mol. Cell Biol. *17,* 426-438

Van Brabant, A.J., Stan, R., and Ellis, N.A. (2000). DNA helicase, genomic instability, and human genetic disease.. Annu. Rev. Genomics Hum. Genet. 1, 409-459.

Bragantini, B., Tiotiu, D., Rothé, B., Saliou, J.M., Marty, H., Cianférani, S., Charpentier, B., Quinternet, M., and Manival, X. (2016). Functional and Structural Insights of the Zinc-Finger HIT protein family members Involved in Box C/D snoRNP Biogenesis. J. Mol. Biol. *428,* 2488-2506.

Bruel, A.L., Franco, B., Duffourd, Y., Thevenon, J., Jego, L., Lopez, E., Deleuze, J.F., Doummar, D., Giles, R.H., Johnson, C.A., et al. (2017). Fifteen years of research on oral-facial-digital syndromes: From 1 to 16 causal genes. J. Med. Genet. *54,* 371-380.

Burnham, D.R., Kose, H.B., Hoyle, R.B., and Yardimci, H. (2019). The mechanism of DNA unwinding by the eukaryotic replicative helicase. Nat. Commun. *10,* 2159.

Cajanek, L., and Nigg, E.A. (2014). Cep164 triggers ciliogenesis by recruiting Tau tubulin kinase 2 to the mother centriole. Proc. Natl. Acad. Sci. U. S. A. *111,* 2841-2850.

Casar Tena, T., Maerz, L.D., Szafranski, K., Groth, M., Blätte, T.J., Donow, C., Matysik, S., Walther, P., Jeggo, P.A., Burkhalter, M.D., et al. (2019). Resting cells rely on the DNA helicase component MCM2 to build cilia. Nucleic Acids Res. *47,* 134-151.

Chavez, M., Ena, S., Van Sande, J., de Kerchove d'Exaerde, A., Schurmans, S., and Schiffmann, S.N. (2015). Modulation of Ciliary Phosphoinositide Content Regulates Trafficking and Sonic Hedgehog Signaling Output. Dev. Cell *34,* 338-350.

Cheah, J.J.C., Hahn, C.N., Hiwase, D.K., Scott, H.S., and Brown, A.L. (2017). Myeloid neoplasms with germline DDX41 mutation. Int. J. Hematol. *106,* 163-174.

Chen, B., Doucleff, M., Wemmer, D.E., De Carlo, S., Huang, H.H., Nogales, E., Hoover, T.R., Kondrashkina, E., Guo, L., and Nixon, B.T. (2007). ATP Ground- and Transition States of Bacterial Enhancer Binding AAA+ ATPases Support Complex Formation with Their Target Protein, σ54. Structure *15,* 429-440.

Cheng, W., Hsieh, J., Brendza, K.M., and Lohman, T.M. (2001). E. coli Rep oligomers are required to initiate DNA unwinding in vitro. J. Mol. Biol. *310,* 327-350.

Chester, N., Babbe, H., Pinkas, J., Manning, C., and Leder, P. (2006). Mutation of the Murine Bloom's Syndrome Gene Produces Global Genome Destabilization. Mol. Cell Biol. *26,* 6713-6726.

Chuang, R.Y., Weaver, P.L., Liu, Z., and Chang, T.H. (1997). Requirements of the DEAD-box protein Ded1p for messenger RNA translation. Science *275,* 1468-1471.

Chung, W.Y., and Chung, L.P. (1999). A case of oral-facial-digital syndrome with overlapping manifestations of type V and type VI: A possible new OFD syndrome. Pediatr.

Radiol. *29,* 268-271.

Corbit, K.C., Shyer, A.E., Dowdle, W.E., Gaulden, J., Singla, V., and Reiter, J.F. (2008). Kif3a constrains β-catenin-dependent Wnt signalling through dual ciliary and non-ciliary mechanisms. Nat. Cell Biol. *10,* 70-76.

Cordin, O., Tanner, N.K., Doère, M., Linder, P., and Banroques, J. (2004). The newly discovered Q motif of DEAD-box RNA helicases regulates RNA-binding and helicase activity. EMBO J. *23,* 2478-2487.

Courcelle, J., and Hanawalt, P.C. (2003). RecA-Dependent Recovery of Arrested DNA Replication Forks. Annu. Rev. Genet. *37,* 611-646.

Craft, J.M., Harris, J.A., Hyman, S., Kner, P., and Lechtreck, K.F. (2015). Tubulin transport by IFT is upregulated during ciliary growth by a cilium-autonomous mechanism. J. Cell Biol. *208,* 223-237.

Croteau, D.L., Popuri, V., Opresko, P.L., and Bohr, V.A. (2014). Human RecQ Helicases in DNA Repair, Recombination, and Replication. Annu. Rev. Biochem. *83,* 519-552.

Dehghani-Tafti, S., Levdikov, V., Antson, A.A., Bax, B., and Sanders, C.M. (2019). Structural and functional analysis of the nucleotide and DNA binding activities of the human PIF1 helicase. Nucleic Acids Res. *47,* 3208-3222.

Dillingham, M.S. (2011). Superfamily I helicases as modular components of DNA-processing machines. Biochem. Soc. Trans. *39,* 413-423.

Donmez, I., and Patel, S.S. (2008). Coupling of DNA unwinding to nucleotide hydrolysis in a ring-shaped helicase. EMBO J. *27,* 1718-1726.

Donnai, D., Kerzin-Storrar, L., and Harris, R. (1987). Familial orofaciodigital syndrome type I presenting as adult polycystic kidney disease. J. Med. Genet. *24,* 84-87.

Du, C., Li, D.Q., Li, N., Chen, L., Li, S. Sen, Yang, Y., Hou, M.X., Xie, M.J., and Zheng, Z.D. (2017). DDX5 promotes gastric cancer cell proliferation in vitro and in vivo through mTOR signaling pathway. Sci. Rep. *7,* 42876.

Dubaele, S., De Santis, L.P., Bienstock, R.J., Keriel, A., Stefanini, M., Van Houten, B., and Egly, J.M. (2003). Basal transcription defect discriminates between xeroderma pigmentosum

and trichothiodystrophy in XPD patients. Mol. Cell *11*, 1635-1646.

Echelard, Y., Epstein, D.J., St-Jacques, B., Shen, L., Mohler, J., McMahon, J.A., and McMahon, A.P. (1993). Sonic hedgehog, a member of a family of putative signaling molecules, is implicated in the regulation of CNS polarity. Cell *75*, 1417-1430.

Edgcomb, S.P., Carmel, A.B., Naji, S., Ambrus-Aikelin, G., Reyes, J.R., Saphire, A.C.S., Gerace, L., and Williamson, J.R. (2012). DDX1 is an RNA-dependent ATPase involved in HIV-1 Rev function and virus replication. J. Mol. Biol. *415*, 61-74.

Edwards, R.J., Bentley, N.J., and Carr, A.M. (1999). A Rad3-Rad26 complex responds to DNA damage independently of other checkpoint proteins. Nat. Cell Biol. *1*, 393-398.

Eggenschwiler, J.T., and Anderson, K. V. (2007). Cilia and Developmental Signaling. Annu. Rev. Cell Dev. Biol. *23*, 345-373.

Enemark, E.J., and Joshua-Tor, L. (2006). Mechanism of DNA translocation in a replicative hexameric helicase. Nature *442*, 270-275.

Enuka, Y., Hanukoglu, I., Edelheit, O., Vaknine, H., and Hanukoglu, A. (2012). Epithelial sodium channels (ENaC) are uniformly distributed on motile cilia in the oviduct and the respiratory airways. Histochem. Cell Biol. *137*, 339-353.

Erickson, R.P., and Bodensteiner, J.B. (2007). Oro-facial-digital syndrome IX with severe microcephaly: A new variant in a genetically isolated population. Am. J. Med. Genet. A. *143A*, 3309-3313.

Faily, S., Perveen, R., Urquhart, J., Chandler, K., and Clayton-Smith, J. (2017). Confirmation that mutations in DDX59 cause an autosomal recessive form of oral-facial-digital syndrome: Further delineation of the DDX59 phenotype in two new families. Eur. J. Med. Genet. *60*, 527-532.

Fairman-Williams, M.E., Guenther, U.P., and Jankowsky, E. (2010). SF1 and SF2 helicases: Family matters. Curr. Opin. Struct. Biol. *20*, 313-324.

Fang, J., Kubota, S., Yang, B., Zhou, N., Zhang, H., Godbout, R., and Pomerantz, R.J. (2004). A DEAD box protein facilitates HIV-1 replication as a cellular co-factor of Rev. Virology. *330*, 471-480.

Fang, J., Acheampong, E., Dave, R., Wang, F., Mukhtar, M., and Pomerantz, R.J. (2005). The RNA helicase DDX1 is involved in restricted HIV-1 Rev function in human astrocytes. Virology *336*, 299-307.

Ferrante, M.I., Zullo, A., Barra, A., Bimonte, S., Messaddeq, N., Studer, M., Dollé, P., and Franco, B. (2006). Oral-facial-digital type I protein is required for primary cilia formation and left-right axis specification. Nat. Genet. *38*, 112-117.

Fisher, A.J., Smith, C.A., Thoden, J.B., Smith, R., Sutoh, K., Holden, H.M., and Rayment, I. (1995). X-ray Structures of the Myosin Motor Domain of Dictyostelium discoideum Complexed with MgADP.BeFx and MgADP.AlF4−. Biochemistry *34*, 8960-8972.

Fliegauf, M., Benzing, T., and Omran, H. (2007). When cilia go bad: Cilia defects and ciliopathies. Nat. Rev. Mol. Cell Biol. *8*, 880-893.

Franco, B., and Thauvin-Robinet, C. (2016). Update on oral-facial-digital syndromes (OFDS). Cilia *5*, 12.

Fuller-Pace, F. V. (2006). DExD/H box RNA helicases: Multifunctional proteins with important roles in transcriptional regulation. Nucleic Acids Res. *34*, 4206-4215.

Gai, D., Zhao, R., Li, D., Finkielstein, C. V., and Chen, X.S. (2004). Mechanisms of conformational change for a replicative hexameric helicase of SV40 large tumor antigen. Cell. *119*, 47-60.

Garcia-Gonzalo, F.R., Corbit, K.C., Sirerol-Piquer, M.S., Ramaswami, G., Otto, E.A., Noriega, T.R., Seol, A.D., Robinson, J.F., Bennett, C.L., Josifova, D.J., et al. (2011). A transition zone complex regulates mammalian ciliogenesis and ciliary membrane composition. Nat. Genet. *43*, 776-784.

Gilula, N.B., and Satir, P. (1972). The ciliary necklace a ciliary membrane specialization. J. Cell Biol. *53*, 494-509.

Goetz, S.C., and Anderson, K. V. (2010). The primary cilium: A signalling centre during vertebrate development. Nat. Rev. Genet. *11*, 331-344.

Gogendeau, D., Lemullois, M., Le Borgne, P., Castelli, M., Aubusson-Fleury, A., Arnaiz, O., Cohen, J., Vesque, C., Schneider-Maunoury, S., Bouhouche, K., et al. (2020). MKS-NPHP

module proteins control ciliary shedding at the transition zone. PLoS Biol. *18,* 3000640.

Gómez, O., and Puerto, B. (2017). Cleft lip and palate. In Obstetric Imaging: Fetal Diagnosis and Care, 2nd Edition.

Gonçalves, J., and Pelletier, L. (2017). The ciliary transition zone: Finding the pieces and assembling the gate. Mol. Cells *40,* 243-253.

Gorbalenya, A.E., and Koonin, E. V. (1993). Helicases: amino acid sequence comparisons and structure-function relationships. Curr. Opin. Struct. Biol. *3,* 419-429.

Greber, B.J., Toso, D.B., Fang, J., and Nogales, E. (2019). The complete structure of the human TFIIH core complex. Elife. *8,* 44771

Grifo, J.A., Abramson, R.D., Satler, C.A., and Merrick, W.C. (1984). RNA-stimulated ATPase activity of eukaryotic initiation factors. J. Biol. Chem. *259,* 8648-8654.

Gurrieri, F., Franco, B., Toriello, H., and Neri, G. (2007). Oral-facial-digital syndromes: Review and diagnostic guidelines. Am. J. Med. Genet. *143a,* 3314-3323.

Hartill, V., Szymanska, K., Sharif, S.M., Wheway, G., and Johnson, C.A. (2017). Meckel-Gruber syndrome: An update on diagnosis, clinical management, and research advances. Front. Pediatr. *5,* 244.

Hassounah, N.B., Bunch, T.A., and McDermott, K.M. (2012). Molecular pathways: The role of primary cilia in cancer progression and therapeutics with a focus on hedgehog signaling. Clin. Cancer Res. *18,* 2429-2435.

He, M., Agbu, S., and Anderson, K. V. (2017). Microtubule Motors Drive Hedgehog Signaling in Primary Cilia. Trends Cell Biol. *27,* 110-125.

Herrera-Moyano, E., Moriel-Carretero, M., Montelone, B.A., and Aguilera, A. (2014). The rem Mutations in the ATP-Binding Groove of the Rad3/XPD Helicase Lead to Xeroderma pigmentosum-Cockayne Syndrome-Like Phenotypes. PLoS Genet. *10,* 1004859.

Hildebrandt, F., Benzing, T., and Katsanis, N. (2011). Ciliopathies. N. Engl. J. Med. *364,* 1533-1543.

Honig, A., Auboeuf, D., Parker, M.M., O'Malley, B.W., and Berget, S.M. (2002). Regulation

of Alternative Splicing by the ATP-Dependent DEAD-Box RNA Helicase p72. Mol. Cell. Biol. *22,* 5698-5707.

Hooper, J.E., and Scott, M.P. (2005). Communicating with hedgehogs. Nat. Rev. Mol. Cell Biol. *6,* 306-317.

Horii, T., Ogawa, T., and Ogawa, H. (1980). Organization of the recA gene of Escherichia coli. Proc. Natl. Acad. Sci. U. S. A. *77,* 313-317.

Ingham, P.W., and McMahon, A.P. (2001). Hedgehog signaling in animal development: Paradigms and principles. Genes Dev. *15,* 3059-3087.

Irigoin, F., and L. Badano, J. (2011). Keeping the Balance Between Proliferation and Differentiation:The Primary Cilium. Curr. Genomics. *12,* 285-297.

Jackson, R.N., Lavin, M., Carter, J., and Wiedenheft, B. (2014). Fitting CRISPR-associated Cas3 into the Helicase Family Tree. Curr. Opin. Struct. Biol. *24,* 106-114.

Jankowsky, E. (2011). RNA helicases at work: Binding and rearranging. Trends Biochem. Sci. *36,* 19-29.

Jankowsky, E., and Bowers, H. (2006). Remodeling of ribonucleoprotein complexes with DExH/D RNA helicases. Nucleic Acids Res. *34,* 4181-4188.

Jankowsky, E., and Fairman, M.E. (2007). RNA helicases - one fold for many functions. Curr. Opin. Struct. Biol. *17,* 316-324.

Jarmoskaite, I., and Russell, R. (2011). DEAD-box proteins as RNA helicases and chaperones. Wiley Interdiscip. Rev. RNA. *2,* 135-152.

Jarmoskaite, I., and Russell, R. (2014). RNA Helicase Proteins as Chaperones and Remodelers. Annu. Rev. Biochem. *83,* 697-725.

Johnson, C.A., and Collis, S.J. (2016). Ciliogenesis and the DNA damage response: A stressful relationship. Cilia. *5,* 19.

Jonassen, J.A., Agustin, J.S., Follit, J.A., and Pazour, G.J. (2008). Deletion of IFT20 in the mouse kidney causes misorientation of the mitotic spindle and cystic kidney disease. J. Cell Biol. *183,* 377-384.

Kagawa, R., Montgomery, M.G., Braig, K., Leslie, A.G.W., and Walker, J.E. (2004). The structure of bovine F1-ATPase inhibited by ADP and beryllium fluoride. EMBO J. *23,* 2734-2744.

Kato, H., Oh, S.W., and Fujita, T. (2017). RIG-I-like receptors and type I interferonopathies. J. Interf. Cytokine Res. *37,* 207-213.

Kawaoka, J., Jankowsky, E., and Pyle, A.M. (2004). Backbone tracking by the SF2 helicase NPH-II. Nat. Struct. Mol. Biol. *11,* 526-530.

Kellaris, G., Khan, K., Baig, S.M., Tsai, I.C., Zamora, F.M., Ruggieri, P., Natowicz, M.R., and Katsanis, N. (2018). A hypomorphic inherited pathogenic variant in DDX3X causes male intellectual disability with additional neurodevelopmental and neurodegenerative features. Hum. Genomics. *12,* 11.

Kellner, J.N., and Meinhart, A. (2015). Structure of the SPRY domain of the human RNA helicase DDX1, a putative interaction platform within a DEAD-box protein. Acta Crystallogr. Acta Crystallogr. F. Struct. Biol. Commun. *71,* 1176-1188.

Kikuma, T., Ohtsu, M., Utsugi, T., Koga, S., Okuhara, K., Eki, T., Fujimori, F., and Murakami, Y. (2004). Dbp9p, a member of the DEAD box protein family, exhibits DNA helicase activity. J. Biol. Chem. *279,* 20692-20698.

Kobayashi, T., Kim, S., Lin, Y.C., Inoue, T., and Dynlacht, B.D. (2014). The CP110-interacting proteins talpid3 and cep290 play overlapping and distinct roles in cilia assembly. J. Cell Biol. *204,* 215-229.

Lechtreck, K.F. (2015). IFT-Cargo Interactions and Protein Transport in Cilia. Trends Biochem. Sci. *40,* 765-778.

Lee, J.Y., and Yang, W. (2006). UvrD Helicase Unwinds DNA One Base Pair at a Time by a Two-Part Power Stroke. Cell *127,* 1349-1360.

van der Lelij, P., Chrzanowska, K.H., Godthelp, B.C., Rooimans, M.A., Oostra, A.B., Stumm, M., Zdzienicka, M.Z., Joenje, H., and de Winter, J.P. (2010). Warsaw Breakage Syndrome, a Cohesinopathy Associated with Mutations in the XPD Helicase Family Member DDX11/ChlR1. Am. J. Hum. Genet. *86,* 262-266.

Li, Y., and Hu, J. (2011). Small GTPases and cilia. Protein Cell. *2,* 13-25.

Linder, P., and Jankowsky, E. (2011). From unwinding to clamping ĝ€" the DEAD box RNA helicase family. Nat. Rev. Mol. Cell Biol. *12,* 505-516.

Lindor, N.M., Furuichi, Y., Kitao, S., Shimamoto, A., Arndt, C., and Jalal, S. (2000). Rothmund-Thomson syndrome due to RECQ4 helicase mutations: Report and clinical and molecular comparisons with Bloom syndrome and Werner syndrome. Am. J. Med. Genet. *90,* 223-228.

Lionnet, T., Spiering, M.M., Benkovic, S.J., Bensimon, D., and Croquette, V. (2007). Real-time observation of bacteriophage T4 gp41 helicase reveals an unwinding mechanism. Proc. Natl. Acad. Sci. U. S. A. *104,* 19790-19795.

Liu, Z.-R. (2002). p68 RNA Helicase Is an Essential Human Splicing Factor That Acts at the U1 snRNA-5' Splice Site Duplex. Mol. Cell. Biol. *22,* 5443-5450.

Liu, F., Putnam, A., and Jankowsky, E. (2008a). ATP hydrolysis is required for DEAD-box protein recycling but not for duplex unwinding. Proc. Natl. Acad. Sci. U. S. A. *105,* 20209-20214.

Liu, H., Rudolf, J., Johnson, K.A., McMahon, S.A., Oke, M., Carter, L., McRobbie, A.M., Brown, S.E., Naismith, J.H., and White, M.F. (2008b). Structure of the DNA Repair Helicase XPD. Cell *133,* 801-812.

Lohman, T.M., and Bjornson, K.P. (1996). Mechanisms of Helicase-Catalyzed DNA Unwinding. Annu. Rev. Biochem. *65,* 169-214.

Lohman, T.M., Tomko, E.J., and Wu, C.G. (2008). Non-hexameric DNA helicases and translocases: Mechanisms and regulation. Nat. Rev. Mol. Cell Biol. *9,* 391-401.

Lu, Q., Insinna, C., Ott, C., Stauffer, J., Pintado, P.A., Rahajeng, J., Baxa, U., Walia, V., Cuenca, A., Hwang, Y.S., et al. (2015). Early steps in primary cilium assembly require EHD1/EHD3-dependent ciliary vesicle formation. Nat. Cell Biol. *17,* 228-240.

Lucius, A.L., Maluf, N.K., Fischer, C.J., and Lohman, T.M. (2003). General methods for analysis of sequential "n-step" kinetic mechanisms: Application to single turnover kinetics of helicase-catalyzed DNA unwinding. Biophys. J. *85,* 2224-2239.

Mackintosh, S.G., and Raney, K.D. (2006). DNA unwinding and protein displacement by superfamily 1 and superfamily 2 helicases. Nucleic Acids Res. *34,* 4154-4159.

Magnusdottir, A., Johansson, I., Dahlgren, L.G., Nordlund, P., and Berglund, H. (2009). Enabling IMAC purification of low abundance recombinant proteins from E. coli lysates. Nat. Methods. *6,* 477-478.

Malicki, J.J., and Johnson, C.A. (2017). The Cilium: Cellular Antenna and Central Processing Unit. Trends Cell Biol. *27,* 126-140.

Mallam, A.L., Del Campo, M., Gilman, B., Sidote, D.J., and Lambowitz, A.M. (2012). Structural basis for RNA-duplex recognition and unwinding by the DEAD-box helicase Mss116p. Nature. *490,* 121-125.

Manosas, M., Xi, X.G., Bensimon, D., and Croquette, V. (2010). Active and passive mechanisms of helicases. Nucleic Acids Res. *38,* 5518-5526.

Marigo, V., Roberts, D.J., Lee, S.M.K., Tsukurov, O., Levi, T., Gastier, J.M., Epstein, D.J., Gilbert, D.J., Copeland, N.G., Seidman, C.E., et al. (1995). Cloning, expression, and chromosomal location of SHH and IHH: Two human homologues of the drosophila segment polarity gene hedgehog. Genomics. *28,* 44-51.

Mashtalir, N., D'Avino, A.R., Michel, B.C., Luo, J., Pan, J., Otto, J.E., Zullow, H.J., McKenzie, Z.M., Kubiak, R.L., St. Pierre, R., et al. (2018). Modular Organization and Assembly of SWI/SNF Family Chromatin Remodeling Complexes. Cell. *175,* 1272-1288.

Mojumdar, A., De March, M., Marino, F., and Onesti, S. (2017). The human RecQ4 helicase contains a functional RecQ C-terminal region (RQC) that is essential for activity. J. Biol. Chem. *292,* 4176-4184.

Mossey, P.A., Little, J., Munger, R.G., Dixon, M.J., and Shaw, W.C. (2009). Cleft lip and palate. Lancet. *374,* 1773-1785.

Müller-Tidow, C., Diederichs, S., Thomas, M., and Serve, H. (2004). Genome-wide screening for prognosis-predicting genes in early-stage non-small-cell lung cancer. Lung Cancer *45,* 145-150.

Mullor, J.L., and Guerrero, I. (2000). A gain-of-function mutant of patched dissects different

responses to the Hedgehog gradient. Dev. Biol. *228,* 211-224.

Nachury, M. V., Seeley, E.S., and Jin, H. (2010). Trafficking to the Ciliary Membrane: How to Get Across the Periciliary Diffusion Barrier? Annu. Rev. Cell Dev. Biol. *26,* 59-87.

Nishijo, K., Nakayama, T., Aoyama, T., Okamoto, T., Ishibe, T., Yasura, K., Shima, Y., Shibata, K.R., Tsuboyama, T., Nakamura, T., et al. (2004). Mutation analysis of the RECQL4 gene in sporadic osteosarcomas. Int. J. Cancer *111,* 367-372.

Nüsslein-volhard, C., and Wieschaus, E. (1980). Mutations affecting segment number and polarity in drosophila. Nature *287,* 795-801.

O'Driscoll, M., Ruiz-Perez, V.L., Woods, C.G., Jeggo, P.A., and Goodship, J.A. (2003). A splicing mutation affecting expression of ataxia-telangiectasia and Rad3-related protein (ATR) results in Seckel syndrome. Nat. Genet. *33,* 497-501.

Otto, E.A., Loeys, B., Khanna, H., Hellemans, J., Sudbrak, R., Fan, S., Muerb, U., O'Toole, J.F., Helou, J., Attanasio, M., et al. (2005). Nephrocystin-5, a ciliary IQ domain protein, is mutated in Senior-Loken syndrome and interacts with RPGR and calmodulin. Nat. Genet. *37,* 282-288.

Pang, P.S., Jankowsky, E., Planet, P.J., and Pyle, A.M. (2002). The hepatitis C viral NS3 protein is a processive DNA helicase with cofactor enhanced RNA unwinding. EMBO J. *21,* 1168-1176.

Parsyan, A., Svitkin, Y., Shahbazian, D., Gkogkas, C., Lasko, P., Merrick, W.C., and Sonenberg, N. (2011). MRNA helicases: The tacticians of translational control. Nat. Rev. Mol. Cell Biol. *12,* 235-245.

Patel, S.S., and Donmez, I. (2006). Mechanisms of helicases. J. Biol. Chem.

Pause, A., Méthot, N., and Sonenberg, N. (1993). The HRIGRXXR region of the DEAD box RNA helicase eukaryotic translation initiation factor 4A is required for RNA binding and ATP hydrolysis. Mol. Cell. Biol. *13,* 6789-6798.

Payne, M., and Hickson, I.D. (2009). Genomic instability and cancer: Lessons from analysis of Bloom's syndrome. Bio. Soc. Trans. *37,* 553-559.

Pedersen, L.B., and Rosenbaum, J.L. (2008). Intraflagellar Transport (IFT) role in ciliary

assembly, resorption and signalling. Curr. Top. Dev. Biol. *85,* 23-61.

Pedersen, L.B., Schrøder, J.M., Satir, P., and Christensen, S.T. (2012). The ciliary cytoskeleton. Compr. Physiol. *2,* 779-803.

Polprasert, C., Schulze, I., Sekeres, M.A., Makishima, H., Przychodzen, B., Hosono, N., Singh, J., Padgett, R.A., Gu, X., Phillips, J.G., et al. (2015). Inherited and Somatic Defects in DDX41 in Myeloid Neoplasms. Cancer Cell *27,* 658-670.

Pugacheva, E.N., Jablonski, S.A., Hartman, T.R., Henske, E.P., and Golemis, E.A. (2007). HEF1-Dependent Aurora A Activation Induces Disassembly of the Primary Cilium. Cell *129,* 1351-1363.

Py, B., Higgins, C.F., Krisch, H.M., and Carpousis, A.J. (1996). A DEAD-box RNA helicase in the Escherichia coli RNA degradosome. Nature *381,* 169-172.

Quesada, A.E., Routbort, M.J., DiNardo, C.D., Bueso-Ramos, C.E., Kanagal-Shamanna, R., Khoury, J.D., Thakral, B., Zuo, Z., Yin, C.C., Loghavi, S., et al. (2019). DDX41 mutations in myeloid neoplasms are associated with male gender, TP53 mutations and high-risk disease. Am. J. Hematol. *94,* 757-766.

Ray, B.K., Lawson, T.G., Kramer, J.C., Cladaras, M.H., Grifo, J.A., Abramson, R.D., Merrick, W.C., and Thach, R.E. (1985). ATP-dependent unwinding of messenger RNA structure by eukaryotic initiation factors. J. Biol. Chem. *260,* 7651-7658.

Roberson, E.C., Dowdle, W.E., Ozanturk, A., Garcia-Gonzalo, F.R., Li, C., Halbritter, J., Elkhartoufi, N., Porath, J.D., Cope, H., Ashley-Koch, A., et al. (2015). TMEM231, mutated in orofaciodigital and Meckel syndromes, organizes the ciliary transition zone. J. Cell Biol. *209,* 129-142.

Robertson-Anderson, R.M., Wang, J., Edgcomb, S.P., Carmel, A.B., Williamson, J.R., and Millar, D.P. (2011). Single-molecule studies reveal that DEAD box protein DDX1 promotes oligomerization of HIV-1 rev on the rev response element. J. Mol. Biol. *410,* 959-971.

Rohatgi, R., and Scott, M.P. (2007). Patching the gaps in Hedgehog signalling. Nat. Cell Biol. *9,* 1005-1009.

Rosenbaum, J.L., and Witman, G.B. (2002). Intraflagellar transport. Nat. Rev. Mol. Cell Biol.

3, 813-825.

Rozen, F., Edery, I., Meerovitch, K., Dever, T.E., Merrick, W.C., and Sonenberg, N. (1990). Bidirectional RNA helicase activity of eucaryotic translation initiation factors 4A and 4F. Mol. Cell. Biol. *10,* 1134-1144.

Rudolf, J., Makrantoni, V., Ingledew, W.J., Stark, M.J.R., and White, M.F. (2006). The DNA Repair Helicases XPD and FancJ Have Essential Iron-Sulfur Domains. Mol. Cell *23,* 801-808.

Salpietro, V., Efthymiou, S., Manole, A., Maurya, B., Wiethoff, S., Ashokkumar, B., Cutrupi, M.C., Dipasquale, V., Manti, S., Botia, J.A., et al. (2018). A loss-of-function homozygous mutation in DDX59 implicates a conserved DEAD-box RNA helicase in nervous system development and function. Hum. Mutat. *39,* 187-192.

Sánchez, I., and Dynlacht, B.D. (2016). Cilium assembly and disassembly. Nat. Cell Biol. *18,* 711-717.

Sarkar, M., and Ghosh, M.K. (2016). DEAD box RNA helicases: Crucial regulators of gene expression and oncogenesis. Front. Biosci. *21,* 225-250.

Sarlós, K., Gyimesi, M., and Kovács, M. (2012). RecQ helicase translocates along single-stranded DNA with a moderate processivity and tight mechanochemical coupling. Proc. Natl. Acad. Sci. U. S. A. *109,* 9804-9809.

Satir, P., and Christensen, S.T. (2007). Overview of Structure and Function of Mammalian Cilia. Annu. Rev. Physiol. *69,* 377-400.

Schlierf, M., Wang, G., Chen, X.S., and Ha, T. (2019). Hexameric helicase G40P unwinds DNA in single base pair steps. Elife *8,* 42001.

Schmidt, K.N., Kuhns, S., Neuner, A., Hub, B., Zentgraf, H., and Pereira, G. (2012). Cep164 mediates vesicular docking to the mother centriole during early steps of ciliogenesis. J. Cell Biol. *199,* 1083-1101.

Scolari, F., Valzorio, B., Carli, O., Vizzardi, V., Costantino, E., Grazioli, L., Bondioni, M.P., Savoldi, S., and Maiorca, R. (1997). Oral-facial-digital syndrome type I: An unusual cause of hereditary cystic kidney disease. Nephrol. Dial. Transplant *12,* 1247-1250.

Sébert, M., Passet, M., Raimbault, A., Rahmé, R., Raffoux, E., De Fontbrune, F.S., Cerrano, M., Quentin, S., Vasquez, N., Da Costa, M., et al. (2019). Germline DDX41 mutations define a significant entity within adult MDS/AML patients. Blood *134,* 1441-1444.

Sengoku, T., Nureki, O., Nakamura, A., Kobayashi, S., and Yokoyama, S. (2006). Structural Basis for RNA Unwinding by the DEAD-Box Protein Drosophila Vasa. Cell *125,* 287-300.

Shamseldin, H.E., Rajab, A., Alhashem, A., Shaheen, R., Al-Shidi, T., Alamro, R., Al Harassi, S., and Alkuraya, F.S. (2013). Mutations in DDX59 implicate RNA helicase in the pathogenesis of orofaciodigital syndrome. Am. J. Hum. Genet. *93,* 555-560.

Shin, S., Rossow, K.L., Grande, J.P., and Janknecht, R. (2007). Involvement of RNA helicases p68 and p72 in colon cancer. Cancer Res. *67,* 7572-7578.

Siebert, J.R. (2007). The oral-facial-digital syndromes. Handb. Clin. Neurol. *87,* 341-351.

Siitonen, H.A., Kopra, O., Kääriäinen, H., Haravuori, H., Winter, R.M., Säämänen, A.M., Peltonen, L., and Kestilä, M. (2003). Molecular defect of RAPADILINO syndrome expands the phenotype spectrum of RECQL diseases. Hum. Mol. Genet. *12,* 2837-2844.

Singla, V., Romaguera-Ros, M., Garcia-Verdugo, J.M., and Reiter, J.F. (2010). Ofd1, a Human Disease Gene, Regulates the Length and Distal Structure of Centrioles. Dev. Cell. *18,* 410-424.

Singleton, M.R., Sawaya, M.R., Ellenberger, T., and Wigley, D.B. (2000). Crystal structure of T7 gene 4 ring indicates a mechanism for sequential hydrolysis of nucleotides. Cell *101,* 589-600.

Singleton, M.R., Dillingham, M.S., and Wigley, D.B. (2007). Structure and Mechanism of Helicases and Nucleic Acid Translocases. Annu. Rev. Biochem. *76,* 23-50.

Snijders Blok, L., Madsen, E., Juusola, J., Gilissen, C., Baralle, D., Reijnders, M.R.F., Venselaar, H., Helsmoortel, C., Cho, M.T., Hoischen, A., et al. (2015). Mutations in DDX3X Are a Common Cause of Unexplained Intellectual Disability with Gender-Specific Effects on Wnt Signaling. Am. J. Hum. Genet. *97,* 343-352.

Song, Y., and Brady, S.T. (2015). Post-translational modifications of tubulin: Pathways to functional diversity of microtubules. Trends Cell Biol. *25,* 125-136.

Spalluto, C., Wilson, D.I., and Hearn, T. (2013). Evidence for reciliation of RPE1 cells in late G1 phase, and ciliary localisation of cyclin B1. FEBS Open Bio. *3*, 334–340.

Spassky, N., and Meunier, A. (2017). The development and functions of multiciliated epithelia. Nat. Rev. Mol. Cell Biol. *18,* 423-436.

Stenmark, H., and Olkkonen, V.M. (2001). The Rab GTPase family. Genome Biol. *2,* 3007.

Stepanek, L., and Pigino, G. (2016). Microtubule doublets are double-track railways for intraflagellar transport trains. Science *352,* 721-724.

Stiff, T., Tena, T.C., O'Driscoll, M., Jeggo, P.A., and Philipp, M. (2016). ATR promotes cilia signalling: Links to developmental impacts. Hum. Mol. Genet. *25,* 1574-1587.

Story, R.M., Weber, I.T., and Steitz, T.A. (1992). The structure of the E. coli recA protein monomer and polymer. Nature. *355,* 318-325.

Strigini, M., and Cohen, S.M. (1997). A Hedgehog activity gradient contributes to AP axial patterning of the Drosophila wing. Development *124,* 4697-4705.

Subramanya, H.S., Bird, L.E., Brannigan, J.A., and Wigley, D.B. (1996). Crystal structure of a DExx box DNA helicase. Nature *384,* 379-383.

Sugarman, G.I., Katakia, M., and Menkes, J. (1971). See-saw winking in a familial oral-facial-digital syndrome. Clin. Genet. *2,* 248-254.

Suhasini, A.N., and Brosh, R.M. (2013). Disease-causing missense mutations in human DNA helicase disorders. Mutat. Res. *752,* 138-152.

Swan, M.K., Legris, V., Tanner, A., Reaper, P.M., Vial, S., Bordas, R., Pollard, J.R., Charlton, P.A., Golec, J.M.C., and Bertrand, J.A. (2014). Structure of human Bloom's syndrome helicase in complex with ADP and duplex DNA. Acta Crystallogr. D Biol. Crystallogr. *70,* 1465-1475.

Syed, S., Pandey, M., Patel, S.S., and Ha, T. (2014). Single-Molecule Fluorescence Reveals the Unwinding Stepping Mechanism of Replicative Helicase. Cell Rep. *6,* 1037-1045.

Talwar, T., Vidhyasagar, V., Qing, J., Guo, M., Kariem, A., Lu, Y., Singh, R.S., Lukong, K.E., Wu, Y., and Sung, P. (2017). The DEAD-box protein DDX43 (HAGE) is a dual RNA-

DNA helicase and has a K-homology domain required for full nucleic acid unwinding activity. J. Biol. Chem. *292*, 10429-10443.

Tanner, N.K., and Linder, P. (2001). DExD/H box RNA helicases: From generic motors to specific dissociation functions. Mol. Cell.

Tanner, N.K., Cordin, O., Banroques, J., Doère, M., and Linder, P. (2003). The Q motif: A newly identified motif in DEAD box helicases may regulate ATP binding and hydrolysis. Mol. Cell. *8*, 251-262.

Tanos, B.E., Yang, H.J., Soni, R., Wang, W.J., Macaluso, F.P., Asara, J.M., and Tsou, M.F.B. (2013). Centriole distal appendages promote membrane docking, leading to cilia initiation. Genes Dev. *27*, 163-168.

Tate, G., Satoh, H., Endo, Y., and Mitsuya, T. (2000). Assignment of Desert Hedgehog (DHH) to human chromosome bands 12q12 → q13.1 by in situ hybridization. Cytogenet. Cell Genet. *88*, 93-94.

Thauvin-Robinet, C., Cossée, M., Cormier-Daire, V., Van Maldergem, L., Toutain, A., Alembik, Y., Bieth, E., Layet, V., Parent, P., David, A., et al. (2006). Clinical, molecular, and genotype-phenotype correlation studies from 25 cases of oral-facial-digital syndrome type 1: A French and Belgian collaborative study. J. Med. Genet. *43*, 54-61.

Thomas, S., Legendre, M., Saunier, S., Bessières, B., Alby, C., Bonnière, M., Toutain, A., Loeuillet, L., Szymanska, K., Jossic, F., et al. (2012). TCTN3 mutations cause Mohr-Majewski syndrome. Am. J. Hum. Genet. *91*, 372-378.

Thomsen, N.D., and Berger, J.M. (2009). Running in Reverse: The Structural Basis for Translocation Polarity in Hexameric Helicases. Cell *139*, 523-534.

Tucker, R.W., Pardee, A.B., and Fujiwara, K. (1979). Centriole ciliation is related to quiescence and DNA synthesis in 3T3 cells. Cell *17*, 527-535.

Tutej, N., Tarique, M., and Tutej, R. (2014). Rice SUV3 is a bidirectional helicase that binds both DNA and RNA. BMC Plant Biol. *14*, 283.

Tuteja, N., Tarique, M., Banu, M.S.A., Ahmad, M., and Tuteja, R. (2014). Pisum sativum p68 DEAD-box protein is ATP-dependent RNA helicase and unique bipolar DNA helicase. Plant

Mol. Biol. *85,* 639-651.

Valente, E.M., Logan, C. V., Mougou-Zerelli, S., Lee, J.H., Silhavy, J.L., Brancati, F., Iannicelli, M., Travaglini, L., Romani, S., Illi, B., et al. (2010). Mutations in TMEM216 perturb ciliogenesis and cause Joubert, Meckel and related syndromes. Nat. Genet. *42,* 619-625.

Vannier, J.B., Sarek, G., and Boulton, S.J. (2014). RTEL1: Functions of a disease-associated helicase. Trends Cell Biol. *24,* 416-425.

Velankar, S.S., Soultanas, P., Dillingham, M.S., Subramanya, H.S., and Wigley, D.B. (1999). Crystal structures of complexes of PcrA DNA helicase with a DNA substrate indicate an inchworm mechanism. Cell. *97,* 75-84.

Venema, J., and Tollervey, D. (1999). Ribosome Synthesis in Saccharomyces cerevisiae . Annu. Rev. Genet. *33,* 261-311.

Verheggen, C., Pradet-Balade, B., and Bertrand, E. (2015). SnoRNPs, ZNHIT proteins and the R2TP pathway. Oncotarget *6,* 41399-41400.

Wallingford, J.B., and Mitchell, B. (2011). Strange as it may seem: The many links between Wnt signaling, planar cell polarity, and cilia. Genes Dev. *25,* 201-213.

Wang, L.L., Gannavarapu, A., Kozinetz, C.A., Levy, M.L., Lewis, R.A., Chintagumpala, M.M., Ruiz-Maldanado, R., Contreras-Ruiz, J., Cunniff, C., Erickson, R.P., et al. (2003). Association between osteosarcoma and deleterious mutations in the RECQL4 gene Rothmund-Thomson syndrome. J. Natl. Cancer Inst. *95,* 669-674.

Wang, Y., McMahon, A.P., and Allen, B.L. (2007). Shifting paradigms in Hedgehog signaling. Curr. Opin. Cell Biol. *19,* 159-165.

Westlake, C.J., Baye, L.M., Nachury, M. V., Wright, K.J., Ervin, K.E., Phu, L., Chalouni, C., Beck, J.S., Kirkpatrick, D.S., Slusarski, D.C., et al. (2011). Primary cilia membrane assembly is initiated by Rab11 and transport protein particle II (TRAPPII) complex-dependent trafficking of Rabin8 to the centrosome. Proc. Natl. Acad. Sci. U. S. A. *108,* 2759-2764.

Wiegand, T., Cadalbert, R., Lacabanne, D., Timmins, J., Terradot, L., Böckmann, A., and Meier, B.H. (2019). The conformational changes coupling ATP hydrolysis and translocation

in a bacterial DnaB helicase. Nat. Commun. *10,* 31.

Winkler, G.S., Araújo, S.J., Fiedler, U., Vermeulen, W., Coin, F., Egly, J.M., Hoeijmakers, J.H.J., Wood, R.D., Timmers, H.T.M., and Weeda, G. (2000). TFIIH with inactive XPD helicase functions in transcription initiation but is defective in DNA repair. J. Biol. Chem. *275,* 4258-4266.

Wolski, S.C., Kuper, J., Hänzelmann, P., Truglio, J.J., Croteau, D.L., Van Houten, B., and Kisker, C. (2008). Crystal structure of the FeS cluster-containing nucleotide excision repair helicase XPD. PLoS Biol. *6,* 149

Wong, I.N., Sayers, J.R., and Sanders, C.M. (2013). Characterization of an unusual bipolar helicase encoded by bacteriophage T5. Nucleic Acids Res. *41,* 4587-4600.

Wu, Y. (2012). Unwinding and rewinding: Double faces of helicase? J. Nucleic Acids 2012, 140601.

Wu, C.G., and Spies, M. (2013). Overview: What are helicases? Adv. Exp. Med. Biol. *767,* 1-16.

Wu, H., Zhai, L.T., Chen, P.Y., and Xi, X.G. (2019). DDX43 prefers single strand substrate and its full binding activity requires physical connection of all domains. Biochem. Biophys. Res. Commun. *520,* 594-599.

Xie, F., Wu, C.G., Weiland, E., and Lohman, T.M. (2013). Asymmetric regulation of bipolar single-stranded DNA translocation by the two motors within Escherichia coli RecBCD helicase. J. Biol. Chem. *288,* 1055-1064.

Xie, P., Wang, Y., Liao, Y., Han, Q., Qiu, Z., Chen, Y., and Zuo, X. (2019). MicroRNA-628-5p inhibits cell proliferation in glioma by targeting DDX59. J. Cell. Biochem. *120,* 17293-17302.

Xu, H.Q. (2003). Simultaneously monitoring DNA binding and helicase-catalyzed DNA unwinding by fluorescence polarization. Nucleic Acids Res. *35,* 70.

Yang, Q., Del Campo, M., Lambowitz, A.M., and Jankowsky, E. (2007). DEAD-Box Proteins Unwind Duplexes by Local Strand Separation. Mol. Cell. *28,* 253-263.

Yao, N., Reichert, P., Taremi, S.S., Prosise, W.W., and Weber, P.C. (1999). Molecular views

of viral polyprotein processing revealed by the crystal structure of the hepatitis C virus bifunctional protease-helicase. Structure. *7*, 1353-1363.

Ye, X., Zeng, H., Ning, G., Reiter, J.F., and Liu, A. (2014). C2cd3 is critical for centriolar distal appendage assembly and ciliary vesicle docking in mammals. Proc. Natl. Acad. Sci. U. S. A. *111*, 2164-2169.

Yilmaz, A., Peretz, M., Aharony, A., Sagi, I., and Benvenisty, N. (2018). Defining essential genes for human pluripotent stem cells by CRISPR-Cas9 screening in haploid cells. Nat. Cell Biol. *20*, 610-619.

Yoshimura, S.I., Egerer, J., Fuchs, E., Haas, A.K., and Barr, F.A. (2007). Functional dissection of Rab GTPases involved in primary cilium formation. J. Cell Biol. *178*, 363-369.

You, J., Wang, X., Wang, J., Yuan, B., and Zhang, Y. (2017). DDX59 promotes DNA replication in lung adenocarcinoma. Cell Death Discov. *3*, 16095.

Zeytinoglu, M., Ritter, J., Wheatley, D.N., and Warn, R.M. (1996). Presence of multiple centrioles and primary cilia during growth and early differentiation in the myoblast CO25 cell line. Cell Biol. Int. *20*, 799-807.

License details and the terms and conditions: Licenses of modified figures were obtained from Copyright Clearance Center. The license details and the terms and conditions provided by the journals and Copyright Clearance Center are available on request.